Physics – Uspekhi **65** (4) 355 – 378 (2022)

REVIEWS OF TOPICAL PROBLEMS PACS number: **42.30. – d**

Metalenses for subwavelength imaging

K V Baryshnikova, S S Kharintsev, P A Belov, N A Ustimenko, S A Tretyakov, C R Simovski

DOI: https://doi.org/10.3367/UFNe.2021.03.038952

Contents

1. Introduction **355**

2. Veselago–Pendry pseudolens and Pendry superlens **357**

3. Superlenses based on media with extreme optical anisotropy **362**

3.1 Canalization of near-field images in media consisting of wires; 3.2 Canalization of near-field images in a one-dimensional metamaterial and resonant tunneling in a photonic crystal; 3.3 Canalization of near-field images in a hyperbolic metamaterial; 3.4 Hyperlenses; 3.5 Endoscopes with subwavelength resolution

4. Metalenses with subwavelength focusing and subwavelength resolution based on metasurfaces **368**

4.1 Superresolution using a double metasurface; 4.2 Superresolution using a zone plate for evanescent waves; 4.3 Superresolution via superoscillations

5. Metalenses with subwavelength resolution based on turbid media **374**

6. Discussion **375**

7. Conclusions **376**

References **377**

Abstract. Devices that form an optical image with a subwavelength resolution in real time — metalenses — are considered. Such devices either operate with near optical fields or convert near fields into wave fields. As a result, the spatial resolution of these devices is not limited by the diffraction limit. At the same time, the image is formed at a considerable distance from the object, which distinguishes near-field metalenses from the instruments used in near-field probe microscopy. Metalenses are implemented based on metamaterials or their two-dimensional analogs, metasurfaces. Historically, this line of research was based on the so-called perfect lens, the concept of which did not withstand experimental verification but gave impetus to the development of real metalenses. Depending on the device and principle of operation, metalenses are called either superlenses or hyperlenses.

Keywords: diffraction limit, subwavelength resolution, near field, materials with a negative refractive index, plasmon

K V Baryshnikova [(1, a)], **S S Kharintsev** [(2, b)], **P A Belov** [(1, c)], **N A Ustimenko** [(1, d)], **S A Tretyakov** [(3, e)], **C R Simovski** [(3, f)]
[(1)] ITMO University,
Kronverkskii prosp. 49A, 197101 St. Petersburg, Russian Federation
[(2)] Kazan Federal University, Institute of Physics,
ul. Kremlevskaya 16A, 420008 Kazan, Russian Federation
[(3)] Aalto University, School of Electrical Engineering,
P.O. Box 11000, Aalto, FI-00076, Finland
E-mail: [(a)] k.baryshnikova@metalab.ifmo.ru, [(b)] skharint@gmail.com,
[(c)] belov@metalab.ifmo.ru,
[(d)] nikita.ustimenko@metalab.ifmo.ru,
[(e)] sergei.tretyakov@aalto.fi, [(f)] konstantin.simovski@aalto.fi

Received 26 August 2020, revised 12 March 2021
Uspekhi Fizicheskikh Nauk **192** (4) 386 – 412 (2022)
Translated by V L Derbov

1. Introduction

In optical microscopy, visualization of objects in real time is implemented by focusing light with a lens, which is a transparent dielectric medium limited by two refracting surfaces (Fig. 1a). Due to the finite size of a lens and Abbe diffraction (i.e., the light beam divergence in any medium, including the free space), the transverse size of the focal spot Δ, corresponding to a point source and obeying the Rayleigh criterion, is determined as follows [1]:

$$\Delta \approx 0.61 \frac{\lambda}{\mathrm{NA}}\,, \tag{1}$$

where λ is the wavelength of light, NA is the lens numerical aperture, which (for a nonimmersion lens) equals $\sin \operatorname{arctg}[D/(2f)]$, f is the lens focal length, and D is its transverse dimension. Note that Eqn (1) is derived within the paraxial approximation of the diffraction theory, and for the case of lenses with a very small focal ratio or apodization, this formula is inapplicable [2]. Lenses with a small focal ratio have limited application because of strong aberrations, which cannot be suppressed by usual methods, and spreads the image more significantly than the diffraction. Lenses with apodization, the artificially introduced gradient of the refractive index near the edges, allow removing the Airy circles phenomenon in the field intensity distribution in the image area. In this case, point objects separated by a distance smaller than 0.61λ can be resolved. The apodization effect is sometimes considered equivalent to emulating in Eqn (1) an effective numerical aperture $\mathrm{NA} > 1$ (sometimes leading to misunderstanding and erroneous results). However, the effect of apodization is relatively small. The diffraction is considered to set a lower bound on the image size of a point source (the Airy circle), approximately equal to $\lambda/2$ (for nonimmersion optics) [3]. Actually, this is not quite so, since in the image area of an extensive object the part of the

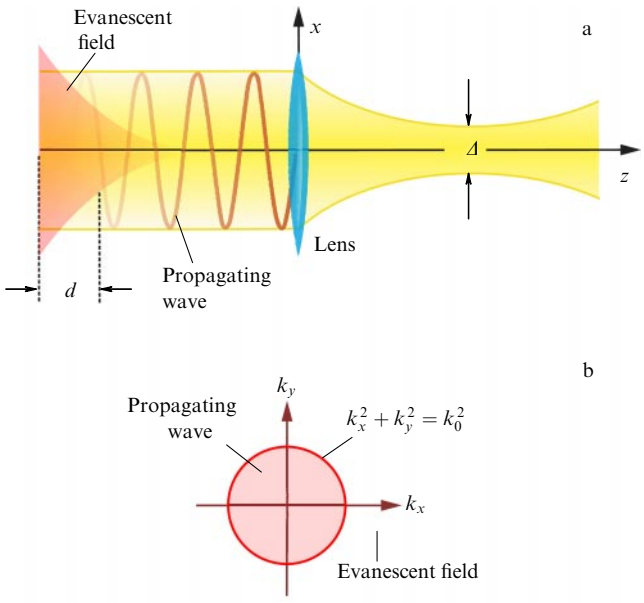

Figure 1. (Color online.) (a) Focusing a propagating electromagnetic wave with a lens. (b) Representation of the electromagnetic wave in two-dimensional k-space.

optical signal that corresponds to its small-scale spatial variations and, correspondingly, evanescent waves are assumed to be completely absent.

The spatial spectrum of radiation (scattering) from any object is a superposition of inhomogeneous (evanescent) and homogeneous (propagating) plane waves. If we take a line connecting a point of the object with the observation point for the z-axis, then, for an unlimited spatial spectrum of the field created by the object, the transverse wave vectors k_x and k_y fill the entire plane in Fig. 1b. For a wave propagating to the observation point ($\mathrm{Im}\, k_z = 0$) with the wave number $k_0 = 2\pi/\lambda$, the spectrum of transverse spatial frequencies is limited by the hatched circle in the figure: $k_z = (k_0^2 - k_x^2 - k_y^2)^{1/2}$, $k_0^2 = k_x^2 + k_y^2$. Beyond this circle, the electromagnetic wave exponentially decays, and this spectrum of spatial frequencies corresponds to evanescent fields. At a distance of approximately $\lambda/2$ from the object, the amplitude of the evanescent wave electric field strength decreases by e times. Thus, free space or the lens material acts as a low-pass filter of the spatial frequency spectrum. Therefore, evanescent fields were not taken into account when deriving Eqn (1). In other words, their fields in the region of the image are assumed to be lower than the noise level. However, upon reducing all optical noises in the system, including the infrared (thermal) ones, evanescent waves can be detected in a special microscope, which allows increasing the resolution level to $\lambda/\Delta \gg 1$. In this case, the resolution limit is actually determined by the level of noise in the microscope [4].

The present review concerns the most frequent case when the optical noise in a microscope cannot be reduced and, nevertheless, it is required to get a subwavelength image in real time without using fluorescent markers or mathematical processing of optical signals. Multiple applications, to which these limitations are relevant, are mentioned in review [5]. So that to implement such image historically first metalenses were created at the beginning of the 21st century, and applying this term to focusing metasurfaces appeared in some papers quite recently. In recent review [6], metalenses based on metasurfaces, aimed at conventional focusing of light, restricted by the diffraction limit, are described in detail.

Note that, long time before the appearance of metalenses, it was understood that, to improve the spatial resolution in absolute values, it is necessary to increase the circle radius k_0 by either reducing the wavelength λ (which is why the short-wave visible or even ultraviolet (UV) range is used in practice) or increasing the refractive index of the medium between the lens and the image (immersion optics). Moreover, in Ref. [7], as long ago as 1928, a local broadening of the spatial frequency spectrum using an optical nanoantenna (probe) or a subwavelength aperture in a metallic screen was proposed, as shown in Fig. 2. In this case, the broadening of the spatial frequency spectrum follows from the uncertainty principle $\Delta x \Delta k_x \sim \mathrm{const}$.

It should be noted that the scattered light detected by a remote detector contains frequencies k_x and k_y only within the circle in Fig. 1b. The main drawback of this method is the necessity to scan the sample surface with a nanoparticle or a subwavelength aperture in the optical near-field region.

Direct access to high transverse spatial frequencies, $k_x^2 + k_y^2 > k_0^2$, in the far field is possible using the wave mixing technique at the expense of the so-called moiré pattern effect (in Section 5, we will briefly mention metalenses using this effect). Such metalenses also require point-by-point scanning of the near field in the sample plane. From this point of view, nanoantenna methods [7] and the moiré pattern method are close to probing (near-field) methods of imaging. In the latter, the subwavelength spatial resolution is ensured by the *a priori* known lateral or axial position of the probe, which is controlled by a piezoelectric scanner with a precision of 0.1 nm for the distance between the probe and the surface of the sample. The interaction of the sample with the localized light allows overcoming the diffraction limit only in the near-field zone, whereas in the far field the scattered light inevitably experiences diffraction, so that a very slow scanning process is inevitable.

The techniques based on reducing the focal volume (or narrowing the point spread function) and its scanning over the sample include a wide class of methods of subwavelength imaging, such as scanning near-field optical microscopy (SNOM) [8, 9], tip-enhanced Raman scattering, (TERS) [10–13], and localized infrared (IR) microscopy (nanoIR) [14, 15]. In 2019, a spatial resolution of $\lambda/1000$ was first demonstrated in the optical range by means of visualizing normal vibrational modes of a single porphyrin molecule using TERS microscopy [16]. Such unprecedentedly high spatial resolution became possible due to the resonance interaction of molecular vibration modes with localized plasmon oscillations of a slit resonator.

In wide-field optical microscopy, the diffraction limit can be overcome without using a nanoprobe by means of mathematical processing of an array of images. Examples are photoactivated localization microscopy (PALM) [17], stochastic optical reconstruction microscopy (STORM) [18], and structured illumination microscopy (SIM) [19]. Finally, subwavelength imaging is implemented without a nanoprobe or secondary processing of optical signals using fluorescence microscopy, in which a spatially nonuniform stimulated emission depletion (STED) of fluorescent markers takes place on the object surface [20, 21].

Below, we will not consider these lines of study, because this review is devoted to metalenses, providing subwavelength

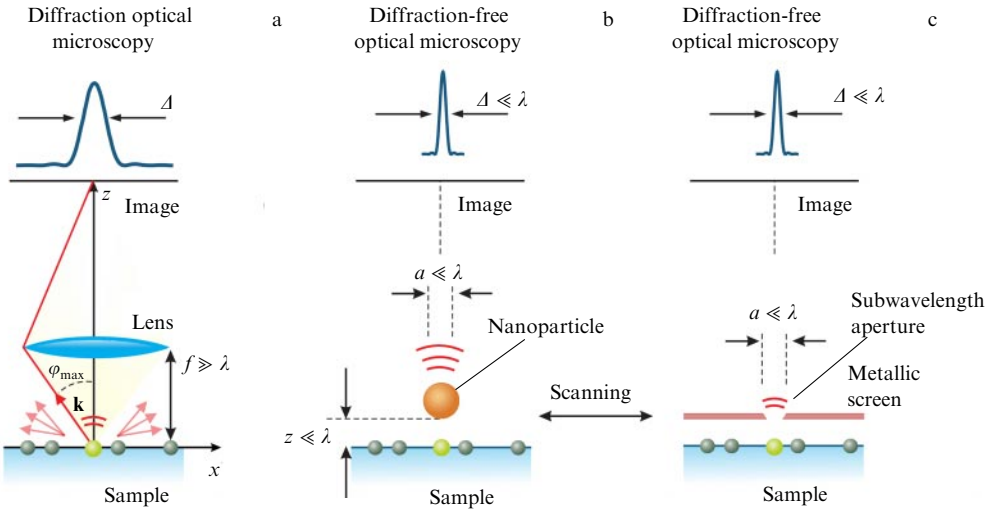

Figure 2. (Color online.) (a) Demonstration of traditional optical microscopy, (b) and (c) schematics of diffraction-free optical microscopy based on a nanoparticle and a subwavelength aperture, respectively.

resolution, i.e., devices that image an object in the far or near wave zones without using probe scanning, fluorescence, nonlinear optical effects, or mathematical processing of data arrays.

2. Veselago–Pendry pseudolens and Pendry superlens

In 1944, L I Mandelshtam (Fig. 3) introduced the notion of backward waves, electromagnetic waves in which the group and phase velocities are oppositely directed. Such waves propagate in a hypothetical medium with a negative refractive index, $n < 0$ [22]. In the case of oblique incidence on an interface separating such a medium from free space or a dielectric, the refraction angle obeys Snell's law and, therefore, turns out to be negative. In 1957, D V Sivukhin proved that Mandelshtam's mode of backward waves takes place in a medium with $\varepsilon < 0$ and $\mu < 0$, where ε and μ are the relative permittivity and permeability, respectively [23].

In 1967, V G Veselago (who, according to our data, did not know about papers [22, 23]) not only presented his own original proof of the fact that a medium with $\varepsilon < 0$ and $\mu < 0$ has a negative refractive index but also systematically studied a number of optical phenomena in such a medium [24]. In his paper [24], the inversion of the Doppler frequency shift and the inversion of Vavilov–Cherenkov emission were predicted, as was the transformation of light pressure into light attraction. However, the concept of the aberration-free pseudolens appeared to be the most fruitful result of this study.

The Veselago pseudolens is a plane-parallel plate of a medium with $n = -1$ and sufficient thickness d. This plate is not a focusing lens, since it does not focus a beam of parallel rays incident on it. At a distance of $d/2$ from the back surface, it focuses only the rays that come from sources located at the same distance from its front surface. No other sources produce images in this plane. In addition, due to the dispersion of the medium with a negative refractive index, the image formation by such a plate is frequency selective.

In practice, the above properties mean suppression of the background illumination of the useful image by objects located either far from the plate or too close to it, as well as all parasitic images when using artificial light directed to the

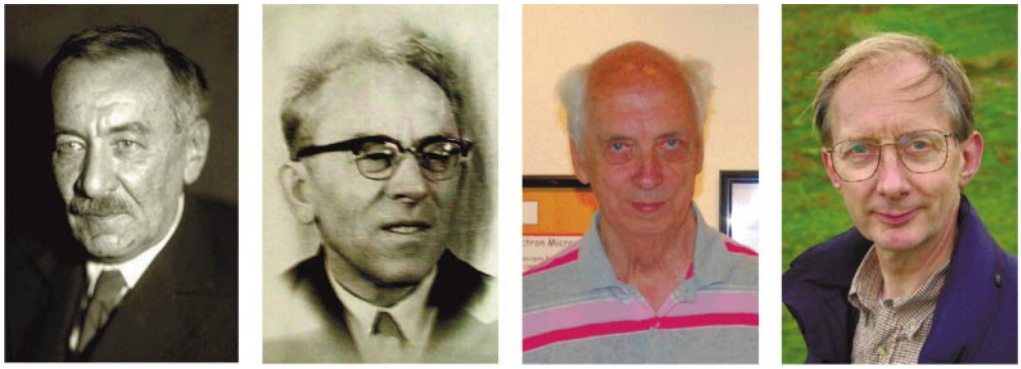

Leonid Isaakovich Mandelshtam
Lebedev Physical Institute
(4.05.1879 – 27.10.1944)

Dmitry Vasil'evich Sivukhin
Moscow Institute of Physics and Technology
(18.08.1914 – 25.10.1988)

Victor Georgievich Veselago
Prokhorov Institute of General Physics of RAS
(13.06.1929 – 15.09.2018)

John Pendry
Imperial College London
(04.07.1942)

Figure 3. Founders of modern electrodynamics of materials with a negative refractive index.

given region of objects. In applied optics, such an image is called pseudoscopic; that is why Veselago called his plate a pseudolens.

Conventional pseudolenses are formed by arrays of microlenses, whose frequency selectivity is achieved either using a resonance substrate (in the 1960s), or by submicron profiling of each microlens (at present). Unfortunately, usual pseudolenses with all their selectivity cannot image an object without aberrations, and the suppression of aberrations requires further complication of the optical system.

The most important advantage of the Veselago pseudolens is the primordial absence of aberrations, as well as of the reflection of waves; a medium with $n = -1$ has the same wave impedance as the free space. Therefore, rays do not undergo refraction when crossing the interfaces between the media, and their beams do not lose homocentricity.

In 2000, J Pendry [25] showed that the Veselago pseudolens not only removes aberrations but also overcomes the diffraction limit of resolution. This happens due to the effect of a resonant increase in the amplitude of evanescent waves, $k_x^2 + k_y^2 > k_0^2$, in a medium with $\varepsilon < 0$ and $\mu < 0$ in the direction away from the source. Such an increase does not contradict conservation laws, because an evanescent wave does not carry energy. Pendry showed that, in the limit of $\varepsilon \to -1$ and $\mu \to -1$, the Fresnel reflection and transmission coefficients for a transverse electric (TE (s)) and transverse magnetic (TM (p)) polarized evanescent wave propagating trough a plane-parallel plate with thickness d (Fig. 4a) has the form [25]

$$\lim_{\substack{\varepsilon\to -1\\ \mu\to -1}} R^{(\mathrm{s,p})} = 0, \quad \lim_{\substack{\varepsilon\to -1\\ \mu\to -1}} T^{(\mathrm{s,p})} = \exp\left(-\mathrm{i}k_z d\right). \tag{2}$$

Since an evanescent wave has a purely imaginary k_z, the wave exponentially increases with distance from the source inside the medium layer, which completely compensates for its decay in the free space at all spatial frequencies (k_x, k_y) such that $k_x^2 + k_y^2 > k_0^2$. Therefore, in contrast to a conventional lens, a Pendry metalens in the image region creates a field in which the contributions of propagating and evanescent waves have a similar order of magnitude, just as in the optical near field. According to Pendry's theory, this is a necessary and sufficient condition for nondiffractive imaging.

Thus, the Veselago pseudolens turns out to be a perfect lens for objects separated by a distance $l < d$ from the front surface of the layer, the image being formed at a distance of $d - l$ from the back surface, as shown in Fig. 4a.

A rigorous solution to the problem of exciting a Veselago–Pendry lens with a point source can be obtained assuming that the lens has nonzero losses (see, e.g., [26, § 4.5.3]). An analysis of the exact solution shows that, when the losses tend to zero, the field distribution in the focal plane of the pseudolens and at greater distances from it tends to a perfect image of the source. However, the field in the region between the pseudolens surface and the image plane (Fig. 4a) is quite different from the object field. This means that a perfect Pendry lens does not create a three-dimensional image of the object. Moreover, when the losses tend to zero, the field inside the lens and in the region of the image becomes singular. This singularity is nonintegrable, so that the reactive energy stored in a perfect pseudolens tends to infinity. We conclude that, in the ideal case considered by Pendry, no physically acceptable solution to the problem exists (see, e.g., [27, 28]). It is interesting that, as Ref. [27] shows, a nonsingular solution

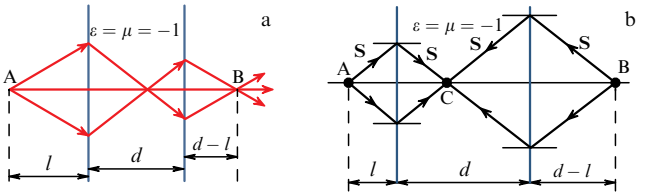

Figure 4. (a) Formation of a perfect image of point object A by a Veselago pseudolens in the Pendry theory. If there are no losses and the relative permittivity and permeability of the Veselago medium remain $\varepsilon = -1$ and $\mu = -1$ for all spatial frequencies of the field created by the object, then there is no diffraction and point object A is imaged by point B. Fields of spatial harmonics corresponding to the evanescent part of the spatial spectrum are reproduced without distortions, since the damping of each evanescent wave in free space is compensated by its growth in the medium layer. (b) Introducing an additional source at point B and a sink at point C [27] allows elimination of the singularity inherent in Pendry's solution. **S** is the Poynting vector.

can be constructed by placing an additional source at the focal point and a point sink at the intermediate focus inside the lens, as shown in Fig. 4b.

In addition, Pendry proposed in [25] an idea for a relatively simple implementation of a superlens (for a single polarization of the waves), which is a thin perfectly uniform layer of a material with $\varepsilon = -1$ (or $\varepsilon = -\varepsilon_\mathrm{m}$, if the surrounding medium is a dielectric with permittivity ε_m) and $\mu = 1$. Ignoring optical losses, silver is such a material in the near UV range. In the silver superlens theory, disregarding losses, it is stated that the field at the ends of a Hertz dipole normal to a silver layer and placed at a small distance $\delta = d/2$, $d \ll \lambda$ from the layer is almost perfectly reproduced just against the dipole at the same distance d from the back surface of the silver nanofilm. Since the subwavelength details of the object can be identified as Hertz dipoles, upon irradiating the object with TM-polarized light, its details will be reproduced in the form of a symmetrically placed subwavelength image. According to Ref. [25], the shape of an extensive object in such an image can be distorted, but the subwavelength resolution of small-scale details would be ensured.

Pendry's view presented in Ref. [25] was supported in a number of papers, e.g., [29–32]. Indeed, the intensity distribution of evanescent TM-polarized waves in the normal direction from a dipole source in the absence of losses in the case of $\delta = d/2$ is such that, for a wave of any spatial frequency, the intensity at the 'near-field image' point repeats the intensity at the source point, as shown in Fig. 5a. However, this does not mean that the field inside a subwavelength object is perfectly repeated at the 'near-field image' point. First, the condition $\delta = d/2$ restricts the superlens action to planar objects only. Second, even a thin scatterer of a subwavelength size, e.g., a nanodisc, even one illuminated with a TM-polarized wave, produces waves with TE polarization. Finally, the field at any point of such a disc contains contributions from not only evanescent but also the propagating waves. Therefore, to judge the near-field image, one should consider the physics of subwavelength imaging rather than the proportion between the evanescent wave damping in the free space and its gain in silver.

No doubt, this effect is due to the increase in evanescent waves across the silver layer; however, the subwavelength image in the region behind the silver film is not formed the way it is in a perfect lens. A dipole object oriented normally to the layer excites surface plasmon polaritons at the boundaries

of the silver layer, the polariton amplitude on the silver back surface turning out to be greater than on the front one [33, 34].

The spatial spectrum of a polariton wave package is very wide and, therefore, the distribution of electric field intensity in the plane of the layer has a sharp maximum at the dipole axis. For a dipole whose dimensions are much less than d, the effective width of this intensity maximum turns out to be much less than the wavelength. The maximum of the transverse distribution of the field intensity with a width of Δ, created by the point dipole on the back surface of the silver thin layer, is exactly the dipole image. For a silver layer in free space, this width can be estimated with high precision as $\Delta \approx 2\pi d/|\log(\varepsilon''/2)|$, where ε'' denotes the imaginary part of the permittivity of silver [33].

If there were no losses in silver, then Δ would tend to zero, $\Delta \to 0$, and the point dipole would indeed be imaged by a point, but on the back surface of the silver layer rather than at a distance $\delta = d/2$ from it. The distance from the object to the silver layer equal to the layer half-thickness, $\delta = d/2$, turns out to be generally not relevant to the subwavelength imaging in a superlens. Subwavelength imaging, considered to be the spatial resolution of two dipoles separated by much less than λ in the superlens plane, is the best on the back surface of the film, where this resolution is Δ [33, 34]. However, this subwavelength resolution has no practical sense and does not mean the formation of a subwavelength image, since it is impossible to read it out. Near-field high-resolution optical microscopes have probes with a metal-coated side surface; therefore, the interaction of the probe with the metallic film destructs the subwavelength spot, which, therefore, cannot be considered a point object image.

In a real silver superlens, e.g., the one experimentally studied in Ref. [35] and schematically shown in Fig. 5b, the silver nanolayer is located between layers of a dielectric (polymethylmethacrylate) with $\varepsilon_m = -\mathrm{Re}\,\varepsilon$. In this case, the image is formed on the substrate surface, the photoresist layer, having a higher permittivity in the linear regime. Such a layered superlens is characterized by spatial intensity distribution different from that in the original Pendry silver superlens [25, 29–31] placed in a homogeneous medium.

Near-field imaging by any plasmonic superlens (not only Pendry type) is based on the formation by a point object of a plasmon wave packet of subwavelength width called a hot spot. If the hot spot lies on the back surface of the nanolayer (silver, but not only), then, as mentioned above, it is useless for imaging.

However, the presence of dielectric layers in which the hot spot is pulled out from the silver in the normal direction with practically preserved spot size allows using probe microscopy to read out hot spots, which thus can be considered subwavelength images of point objects, the resolution of two point dipoles being approximately equal to the width of the plasmonic spot.

The dielectric layer thickness, separating the silver film from the photoresist, is much smaller than the wavelength, and pulling out the hot spot through the entire thickness of the layer occurs because the near field, produced by the point object, in the region behind the silver film has the polarization mainly normal to it. Therefore, at the photoresist-air interface, a jump of the field occurs, equal to the square of the resist refractive index. Thus, at the photoresist-air interface, a second local maximum of the field appears, which is exactly what explains the hot spot pulling out through the entire width of the photoresist. In this case, the internal reflection of

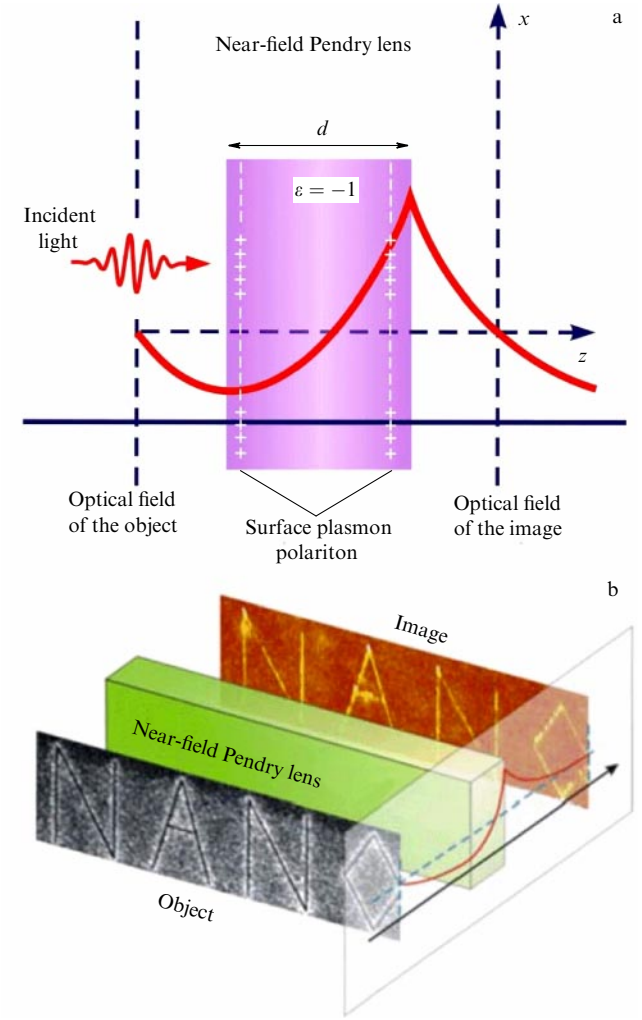

Figure 5. (Color online.) (a) Exponential growth of evanescent wave amplitude in a layer of a medium with $\varepsilon = -1$ and $\mu = 1$ in the theory of a silver superlens is often interpreted as a necessary and sufficient condition for near-field image formation. (b) Experimental demonstration of object visualization with subwavelength details of the order of $\lambda/5$ using a Pendry-type superlens made of silver film [35]. Space between the film and the object and between the film and the image is filled with a dielectric medium and the image is formed on the surface of the photoresist. Total thickness of the dielectric layers is substantially greater than d (Figure 5b from [35] is reproduced courtesy of the American Association for the Advancement of Science; permission received via the Copyright Clearance Center, Inc.)

evanescent waves in the photoresist layer facilitates preserving nearly the same width of the intensity maximum as on the back surface of the silver film.

In the layer superlens considered, the spatial resolution (in both calculations and experiments) reaches a level of $\Delta \approx \lambda/5$, the distance between the source plane to the image plane being nearly the same, and the silver thickness being close to $\lambda/8$ [35]. Of course, this is only a particular result which does not mean that a superlens forms such an image of a point object, whose width is fixed to the wavelength of light incident on the object. In fact, the image width is associated with the surface plasmon wavelength and amounts to a few special such wavelengths. The result $\Delta \approx \lambda/5$ corresponds to the case when the plasmon resonance of the silver layer takes place at a wavelength of $\lambda = 360$ nm.

Other layered superlenses are known in which subwavelength imaging without loss of sharpness can be achieved at a

certain distance from the back surface of the silver nanolayer (see, e.g., review [36]). All of them can be considered Pendry-type superlenses. A general requirement for subwavelength resolution in a Pendry-type superlens is polishing of layer surfaces such that the roughness is less than 1 nm and the deviation of layers from ideally parallel does not exceed a few nanometers within the area of the imaged object. Obviously, expensive nanotechnology is required for this purpose.

Nevertheless, the Pendry-type superlens turned out to be competitive in the production of X-ray diffraction gratings [36]. In this case, expensive nanotechnology is used once to fabricate the parent grating [36]. Somewhat blurred due to the finite plasmon spot width but practically applicable copies of the parent grating are produced in a photoresist using so-called plasmonic lithography, a form of optical lithography, implementing subwavelength resolution. In this case, the parent grating is the imaged object, and the layered structure, consisting of glass, silver, air, and photoresist nanolayers, operates as a superlens. Plasmonic lithography has two obvious advantages over the usual superhigh-resolution contact lithography: it is much cheaper (a few ten times in the case of mass production) and much faster. Using contact lithography, it is possible to fabricate an X-ray diffraction grating with an area of about 1 mm^2 in several hours, whereas plasmonic lithography reproduces a replica of the parent grating of the same area in less than a minute [36].

Note that the implementation of the Veselago pseudolens for propagating waves described in Ref. [24] was confirmed by precise calculations in 1978. In Ref. [37], R A Silin showed through calculations that the waves propagating in a photonic crystal formed by spherical cavities in a medium with $\varepsilon \gg 1$ are backward. Such a discrete medium has an effective refractive index $n = -1$, and a layer of such a medium is an aberration-free pseudolens (we refer to it as a Veselago pseudolens, but to our knowledge, Silin at that time was not aware of Veselago's work and independently reproduced his result on suppressing aberrations). According to Silin's book [38], his group experimentally implemented a plane-parallel pseudolens in the microwave range in the 1980s.

However, for evanescent waves, the photonic crystal formed by spherical inclusions with a period of the order of a wavelength in a matrix, of course, could not be interpreted as a continuous medium with $n = -1$. Therefore, the effect of spatial growth, or at least the absence of a decrease in evanescent waves, which is a key effect for any superlens, cannot be observed in such a structure, either.

As to continuous media with a negative refractive index, they are possible only together with losses: the refractive index is complex, its real part is negative and its imaginary part is nonzero, though small. However, a negative refractive index in the entire infinite frequency range is impossible: both in the static limit and in the limit of frequency tending to infinity it is necessarily positive, as known from textbooks on the electrodynamics of continuous media. For n being negative in a certain frequency range, strong frequency dispersion of ε and μ is required. As follows from the Kramers–Kronig relations, dispersion inevitably leads to optical losses. In magnetic semiconductors, as Veselago found with regret, the condition $\mathrm{Re}\, n = -1$ can be achieved only at the cost of high losses, i.e., $|\mathrm{Im}\, n| > |\mathrm{Re}\, n|$.

When the concept of the perfect Pendry lens appeared at the end of the 20th/beginning of the 21st centuries, the scientific community set a goal to get closer to the perfect image (the fundamental shortcomings of the concept itself had not yet been identified). Therefore, an idea of a metamaterial appeared, i.e., a composite medium with optically small-scale discreteness, such that the material could be considered optically continuous in the working frequency range, not only for propagating waves but also for evanescent waves of sufficiently high frequencies. At the same time, the inclusions in the composite should be such that not only the real part of the refractive index is negative, e.g., $\mathrm{Re}\, n \approx -1$, but also the imaginary part is sufficiently small: $|\mathrm{Im}\, n| \ll |\mathrm{Re}\, n|$.

Since an inhomogeneous medium cannot be effectively continuous over the entire infinite spatial spectrum of evanescent waves and cannot have negligibly small losses in the appropriate frequency region, the perfect Pendry lens concept was replaced with a more realistic concept of a wave superlens. The superlens produces both a far-field image (conformal mapping of an extensive object) and a near-field image (sufficiently fine spatial resolution of small-scale details of the object). It was for this purpose that the first metamaterials were created — their inventors believed in the possibility of implementing such a superlens.

The first metamaterials were optically dense lattices of metallic inclusions in a transparent matrix for experiments in the microwave range. Examples of such composites are shown in Fig. 6. If each inclusion has a response like that of an oscillatory circuit, this is known to correspond to a Lorentzian scattering line and Lorentzian dispersion of electric and magnetic polarizability. Such a response is resonant and narrow-band. If the inclusions possess a collective response, like the plasma one, as, for example, in metals in the infrared (IR) and visible spectral regions of electromagnetic waves, then the response turns out to be broadband.

For metals at optical frequencies, disregarding losses, the permittivity can be presented as a function of frequency using the Drude formula [3]: $\varepsilon(\omega) = 1 - \omega_e^2/\omega^2$, where $\omega_e = \sqrt{n_e e^2/\varepsilon_0 m_{\mathrm{eff}}}$ is the plasma frequency, n_e is the concentration of electrons, and m_{eff} is the effective mass of electrons. Such a response in the microwave region is given by an optically dense periodic lattice of parallel metallic wires (for waves propagating perpendicular to the wires and having the field electric component parallel to them) (Fig. 8a).

Therefore, the historically first metamaterial [39], which demonstrated a negative refractive index in the microwave range for the waves, propagating in a certain plane, consisted of wires perpendicular to this plane, providing $\varepsilon < 0$ for the corresponding waves in a wide range of frequencies, and of resonance magnetic scatterers in the form of double wire split rings that provided $\mu < 0$ in a narrow band of frequencies. Anyway, in spite of the widest resonance inspired by publication [39], this structure turned out to be unsound, even to implement the regime of the Veselago pseudolens. What is more, this material was not an effectively continuous medium for evanescent waves. A review of unsuccessful attempts and analysis of the reasons for failure can be found in reference book [40, Ch. 1]. The main reason for the failures is the high level of losses in subwavelength magnetic resonators, which even in the microwave range does not allow implementing the mode $|\mathrm{Im}\, n| \ll |\mathrm{Re}\, n|$ in the region where $\mathrm{Re}\, n \approx -1$.

In the optical range, the situation of synthesizing a medium having negative permeability is even more complex than for microwaves or millimeter waves. The metamaterial that demonstrated $\mathrm{Re}\, \mu < 0$ at a wavelength of 813 nm [41]

possessed yet higher losses than the first metamaterial [39]. Also, there was no success in attempts to create a magnetic plasma with Drude-type permeability, i.e., $\mu(\omega) = 1 - \omega_m^2/\omega^2$, where ω_m is the analog of plasma frequency for magnetic plasma (an idea of such plasma was proposed in Ref. [42], and attempts were made to synthesize it using both the resonances of plasmon clusters and the magnetic Mie resonance in semiconductor spheres). The point is that a necessary condition for high-frequency artificial magnetism is the presence of a resonance response, and any resonance of an inclusion in a transparent surrounding medium, even the Mie resonance in an almost transparent sphere of crystalline silicon, implies resonance losses in a medium consisting of such inclusions [40].

Thus, the three-dimensional wave Pendry superlens — the practical implementation of a perfect lens — turned out to be unrealizable, and all known metamaterials, to be unable to implement the negative refractive index mode for evanescent waves. This also includes a metamaterial made of disordered wire spirals [43], as shown in Fig. 6b.

At the same time, for propagating waves, the $|\mathrm{Im}\, n| \ll |\mathrm{Re}\, n|$ mode in the region where $\mathrm{Re}\, n \approx -1$, i.e., the mode that allows creating a Veselago pseudolens at optical frequencies, was implemented not long ago (see, e.g., [44, 45]). However, to realize this mode in the near IR range, it is not necessary to use a metamaterial. A photonic crystal of air spheres in a semiconductor matrix successfully copes with this problem (see [46, Ch. 1], as well as [47]).

At the end of this section, let us discuss the experimentally implemented near-field Pendry superlens. About 10 years ago, a practical application was found in the technology of fabricating X-ray diffraction gratings from a photosensitive material, where it is used as a subwavelength concentrator of the electric field generated by the primary X-ray grating illuminated with a UV laser beam. In essence, the silver superlens produces a 1:1-scale image of the primary grating on a photoresist. In this way, it is possible to make a number of replicas of the primary grating in the photoresist. At the same time, all attempts to apply this superlens to imaging structures different from the simplest amplitude grating with an optically small period have been in vain until now. Let us try to understand and discuss the reasons for this failure.

The physical mechanism of subwavelength resolution is related to the excitation of a surface plasmon polariton on both sides of a silver film. At the boundary of the silver, or generally, an interface between a plasmonic metal and a dielectric (Fig. 5a), a surface wave can propagate with the wave vector

$$k_x = k_0 \sqrt{\frac{\varepsilon(\omega)\varepsilon_d}{\varepsilon(\omega) + \varepsilon_d}}, \tag{3}$$

where ε_d is the permittivity. From Eqn (3), it follows that, under the condition $\mathrm{Re}\, \varepsilon(\omega) = -\varepsilon_d$, a resonance takes place, i.e., in the absence of losses, the surface wave can have an infinitely large amplitude. Since the metal permittivity possesses dispersion approximately described by the Drude formula, as well as a nonzero imaginary part, the surface wave amplitude is finite. The proportion of the amplitudes of the surface waves at the sides of the plasmonic metal layer depends on the layer thickness. At some sufficient but not too large a thickness of the layer, it turns out that the surface wave amplitude on the back surface is greater than on the front one. Since the surface wave exponentially decays with the distance from the surface: it is evanescent. The fact that the amplitude of the surface wave is greater at the back surface of the film is nothing more than an increase in the evanescent wave across the layer, similar to that in a perfect Pendry lens. This effect yields a near-field image of the object near the back surface of the layer. The physics of such an increase has an analog in the theory of induced oscillations in a system of two elastically coupled oscillators. It is thoroughly considered in reference book [46, Ch. 1].

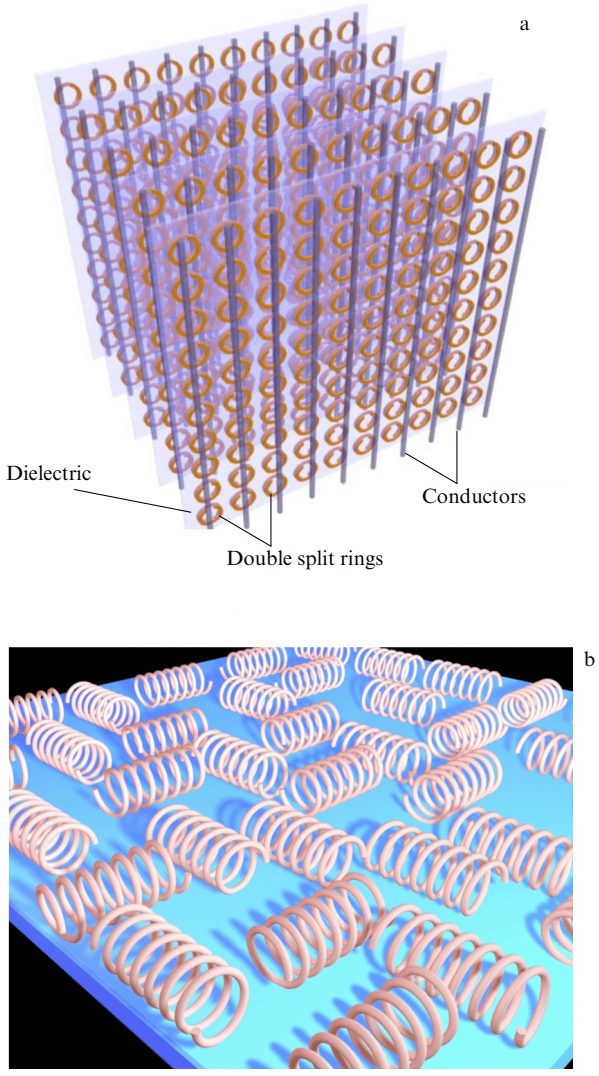

Figure 6. (Color online.) Schematic diagrams of metamaterials with a negative refractive index: (a) combination of metallic rods and double split rings, (b) disordered spirals [43].

The near-field Pendry superlens as an imaging structure has three main drawbacks. First, it does not form a wave image of an extensive object. Second, it forms an image at a very small distance from the object of the order of a quarter of a wavelength (half of this distance being the thickness of the silver film and a half being two similar dielectric gaps between the object and the film and between the film and the probe). The distance from the probe to the object is of the order of $\lambda/4$; if $\lambda = 360$ nm, it does not satisfy the requirements for noninvasive imaging. Finally, the superlens operates in a very narrow band of frequencies. In the analytical loss-free model, surface plasmons are excited at the crossing frequency of the dispersion curves for metal and dielectric permittivities

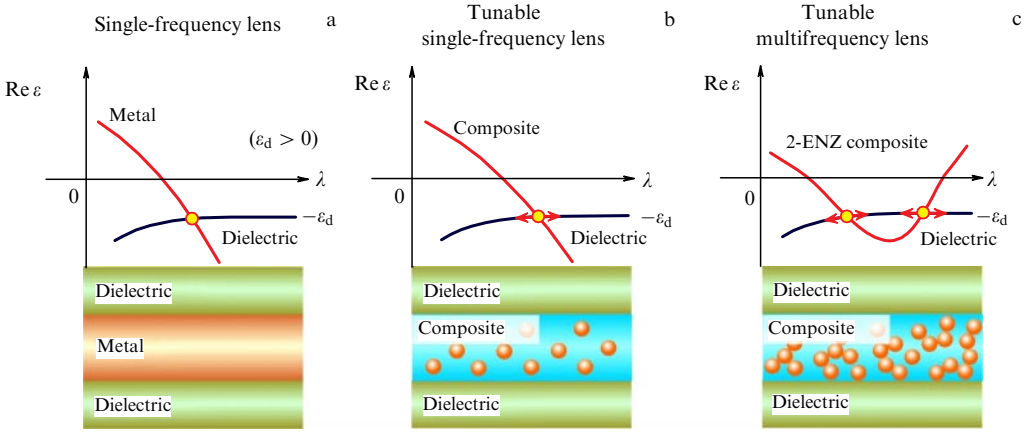

Figure 7. (Color online.) Schematic diagrams of near-field metalenses: (a) single-frequency, (b) tunable single-frequency, and (c) tunable multifrequency [51]. (Figure from Ref. [51] is reproduced courtesy of RSC Pu; permission received via the Copyright Clearance Center, Inc.)

(Fig. 7a). In the rigorous model, the relevant frequency band has a finite nonzero width, which is, however, much less than the signal bandwidth of existing UV lasers.

The excess frequency selectivity of a superlens gives rise to a strong reflection of energy from it. Although evanescent waves do not carry energy, their reflection leads to a loss of energy, because a pair of coherent evanescent waves, arising in the process of reflection, carries energy. Reflections of the spectrum parts beyond the superlens bandwidth substantially reduce the signal in the image region. Therefore, imaging using a silver superlens turns out to be extremely energy inefficient.

Instead of silver, a metal-dielectric composite described by the effective permittivity ε_{eff} [48] can be used. When adding silver nanoparticles to a dielectric matrix with the volume filling factor f ($0 \leqslant f \leqslant 1$), it is possible to find the effective permittivity using the Lorentz–Lorenz formula [49]

$$\varepsilon_{\text{eff}} = \varepsilon_{\text{d}} \frac{1 + 2f\left[(\varepsilon - \varepsilon_{\text{d}})/\varepsilon + 2\varepsilon_{\text{d}}\right]}{1 - f\left[(\varepsilon - \varepsilon_{\text{d}})/\varepsilon + 2\varepsilon_{\text{d}}\right]} . \qquad (4)$$

A numerical estimation using Eqn (4) is valid upon the condition $f < 1/d_{\text{E}}$ (here, d_{E} is the medium dimensionality). Beyond the percolation threshold, $f \geqslant 1/d_{\text{E}}$, a more precise method of extracting the material parameters of the layer from its S-parameters (complex coefficient of reflection and transmission) can be used to model the effective permittivity (see, e.g., [50]). In Ref. [49], the aim of using the nanocomposite instead of silver was the potential to change the operating frequency by varying the parameters of the particles, i.e., to tune the superlens for operation at the wavelength of an existing high-power laser. However, in recent paper [51], it was shown that the use of a nanocomposite also allows widening the frequency band, in which the composite permittivity (more precisely, its real part) is negative.

In the percolation regime, some metal-dielectric composite films exhibit the double-epsilon-near-zero (2-ENZ) behavior of permittivity, as shown in Fig. 7c. This means that the plasmon resonance condition (4) is satisfied for inclusions at two frequencies. In practice, if these frequencies are close to each other, it becomes possible to double the superlens bandwidth, which solves the problem of excess frequency selectivity.

However, this is far from all that the mode of a 2-ENZ medium allows. If a valley of function $\varepsilon_{\text{eff}}(\omega)$ forms, a broad band (frequency continuum) of plasmon excitations can arise. In contrast to plasmon polaritons in usual plasmonic materials, where special schemes of coupling laser light to electronic plasma are required for their excitation, in 2-ENZ metamaterials, the surface plasmon polaritons can be excited by the direct action of light. Moreover, in a wideband valley, the material can behave like a medium with a quasi-zero refractive index, $n \approx 0$, if optical losses are not high. Although a layer of a medium with $n \approx 0$ is not the same as a Pendry superlens, this layer also possesses an ability to form a near-field image, if nonlinear effects are involved, such as stimulated Raman scattering and nonlinear scattering in a random medium (see, e.g., [51–53]).

3. Superlenses based on media with extreme optical anisotropy

3.1 Canalization of near-field images in media consisting of wires

One possible method to overcome the diffraction limit and transmit subwavelength images with a resolution no worse than $\lambda/10$ in the visible and near IR ranges over distances greater than a wavelength is the method of near-field image canalization proposed in 2005 for the microwave range [54]. Later, it was extended to higher frequencies, including optical ones, and many times verified experimentally in various frequency ranges, from microwave to near IR [54–66]. The authors of the proposed method abandoned the use of the evanescent wave amplification effect. As an alternative, they proposed converting evanescent waves into propagating ones. The conversion occurs with high efficiency at the boundary of such a metamaterial, inside which all eigenwaves excited by external sources are propagating.

Actually, external sources at the interface can excite evanescent modes as well, but the latter will not carry energy, since the thickness of the metamaterial layer in such a superlens is much greater than the wavelength. Upon an absence of losses in the metamaterial and correctly chosen layer thickness, the propagating waves will transfer the image from one surface of the lens to another without loss of quality, as if these surfaces were connected by means of an array of subwavelength waveguides (Fig. 8). (In radiophysics, one can easily imagine a dense array of parallel coaxial cables). On the

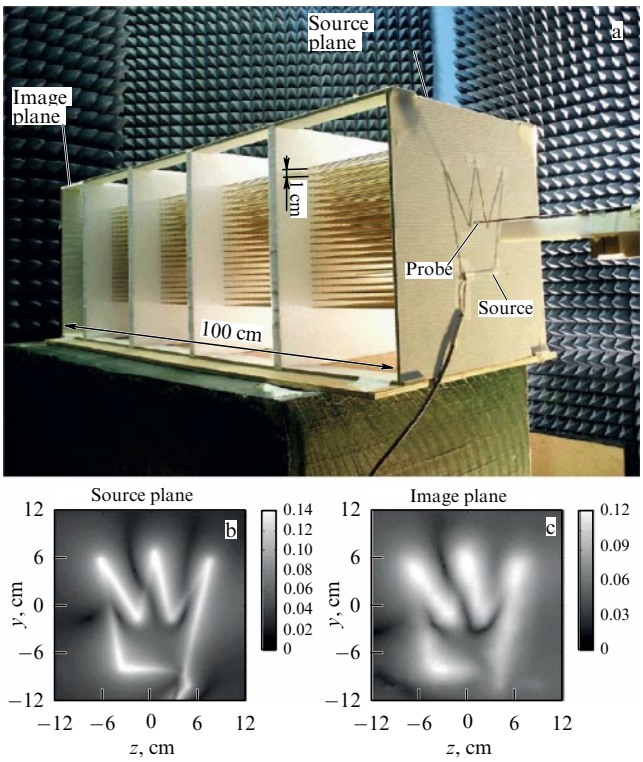

Figure 8. (Color online.) (a) Photo of a superlens based on 21 × 21 wires 1 m long. Radius of each wire is 1 mm. Results of scanning with a near field probe of the source plane (b) and the image plane (c) [66]. (Figure from [66] reproduced courtesy of © American Physical Society 2008.)

back surface of the superlens, the eigenmodes of the metamaterial convert back into evanescent waves, and the image is restored near the back surface.

A very important property of the metamaterial considered is the absence of resonant losses. The near-field image canalization requires the losses to be very small, so that, in this case, the metamaterial properties are due to strong spatial dispersion rather than resonances of inclusions.

Consider the physics of the canalization process in terms of isofrequency. Let us assume that the metamaterial has a flat isofrequency surface, i.e., for a wave propagating along the x-axis, the range is restricted to the infinite band $k_x \leqslant k_0$ rather than the circle $k_x^2 + k_y^2 \leqslant k_0^2$ as for a wave in a vacuum (Fig. 9). Then, a wave with any component k_y of the wave vector will be a propagating wave.

Since the implementation of a flat isofrequency surface requires extreme nonequivalence of the x and y directions, the metamaterial is to be extremely anisotropic. An example of a metamaterial providing an isofrequency surface close to planar in the range from microwave to near IR is the medium of optically thin (but thick compared to the skin layer) metallic wires in a dielectric matrix or vacuum. In the analytical model of a medium consisting of wires in a vacuum, its permittivity tensor is written in the form

$$\hat{\varepsilon} = \begin{pmatrix} \varepsilon_{\parallel} & 0 & 0 \\ 0 & \varepsilon_{\perp} & 0 \\ 0 & 0 & \varepsilon_{\perp} \end{pmatrix}, \tag{5}$$

where the permittivity in the direction perpendicular to the x-axis, along which the wires are stretched, is equal to the relative permittivity of the vacuum, $\varepsilon_{\perp} = 1$, and along the x

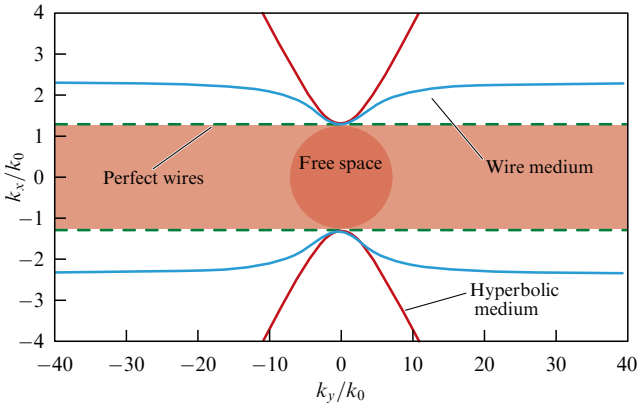

Figure 9. (Color online.) Isofrequency contours in the (k_x, k_y) plane for a medium of silver nanowires in the mid-IR range. Curves are calculated using three analytical models. Solid blue curves are obtained using the exact model taking into account spatial dispersion in the metamaterial (this model has been verified many times numerically and experimentally). Solid red curves are obtained in the model that ignores spatial dispersion, wire medium being erroneously treated as a hyperbolic metamaterial. Green dashed lines correspond to the approximation of perfectly conducting metal for wires. Painted areas correspond to propagating waves (dark red for free space and light red for the medium of perfectly conducting wires). (Figure adapted from Ref. [65]).

direction [67, 68],

$$\varepsilon_{\parallel}(\omega, k_z) = 1 - \frac{\Omega_{\mathrm{p}}^2}{\omega^2 - \delta^2 - c^2 k_x^2}, \tag{6}$$

where Ω_{p} is the effective plasma frequency of a medium consisting of wires, δ corresponds to the absorption in the metal, c is the velocity of light in a vacuum, and ω is the circular frequency of the electromagnetic wave. A metamaterial with such permittivity supports a hyperbolic dispersion regime at frequencies below Ω_{p} (see the solid red line in Fig. 9). For perfectly conducting metals, the absorption tends to zero, then the permittivity along the direction of the wires is described by the simple function $\varepsilon_{\parallel}(\omega, k_z) = 1 - \Omega_{\mathrm{p}}^2/(\omega^2 - c^2 k_x^2)$, which corresponds to a planar isofrequency surface and the existence of special 'waveguide' modes for $|k_x| \leqslant \omega/c$ (see the green dashed line in Fig. 9). For real metals, with the spatial dispersion arising in the wire medium taken into account, the isofrequency curve looks more complicated (see the blue solid line in Fig. 9) [42, 61, 67, 69]. In Fig. 9, the red color highlights the domain of propagating waves (compare with the circular domain for the case of free space in the center of the figure).

At the interface between the superlens (a layer of wire medium) and free space, TM polarized propagating waves refract into the medium and convert into TEM modes propagating along the x-axis (along the wires). Similarly, TM polarized evanescent waves convert into TEM waves and travel with the same phase and group velocities as the propagating ones.

If there is no total reflection at the layer interfaces, the information on the near field distribution is contained in the amplitude and phase distributions of the wave packet. The spatial frequencies of the wave packet are the wavenumbers perpendicular to the x-axis. These spatial frequencies do not determine the phase of group velocities — they determine only the period of spatial harmonics in the yz plane.

Thus, the necessary condition for near-field image canalization is the absence of reflection at the interface between the metamaterial and the environment. This is achieved by choosing the layer thickness, which must be an integer multiple of half the wavelength in the environment medium. Under such a condition, the wire medium operates like an array of noninteracting waveguides, along which the TEM modes propagate (or, more precisely, quasi-TEM modes, due to the presence of optical losses.

The advantages of the canalizing superlens are the following.

(1) Low losses in the metamaterial, i.e., relatively high energy efficiency. At large wire thickness compared to the skin layer thickness, the electromagnetic wave barely penetrates into the wires and weakly decays when propagating along them. Therefore, in superlenses implemented using aluminum or silver nanowires, the energy losses in the superlens are mainly due to the absorption in the matrix surrounding the wires.

(2) Low sensitivity of the image quality to losses. For extremely anisotropic materials, the eigenmode damping is the same over the entire spatial spectrum of the wave packet, which means that the losses reduce the image intensity rather than cause distortions.

(3) Low sensitivity of the images to the precision of material fabrication. Upon small deviations of wire thickness from the mean value, as well as small variations of their relative position, the image formed on the back surface of the superlens stays virtually unchanged, as was shown by experiments.

(4) Large distances through which the images can be canalized. For example, in Ref. [62], it was shown that the image can be transferred through a distance of up to 42 wavelengths in a matrix with a resolution of up to $\lambda/10$. However, to obtain the resolution of $\lambda/25$, the superlens thickness should be reduced to five wavelengths.

The main drawback of the imaging method considered lies in its essence: the image of an object can be obtained only for its surface and only by 'leaning' it against the superlens. The superlens gives no three-dimensional images, and the surface images can be practically obtained only for distances of the order of $\lambda/10$ (or less) from the front surface of the superlens, i.e., in the near-field zone.

A few words about the 'pitfalls' — nonobvious shortcomings of the canalizing superlens. As shown in Refs [56, 70], the reflection from a lens made of extremely anisotropic materials is due to the resonances arising in the 'waveguide' modes inside the structure. Therefore, image transmission with minimum distortions occurs only at wavelengths lying within the band of waveguide modes. Image distortions are possible also because of imperfect transmission of the near-field image through the interface, even if there are no reflections.

The strong spatial dispersion of a wire medium allows the formation of a flat isofrequency surface. In media free of spatial dispersion, isofrequency surfaces are spheres, ellipsoids, or, in the exotic case of a hyperbolic medium, hyperboloids. However, the same strong spatial dispersion limits (in the region of evanescent waves) the spatial frequencies for which the transmission coefficient of the spatial harmonic is equal to one. For harmonics with very large values of $k_y \gg k_0$, the transmission coefficient is substantially different from one. From these considerations, it is possible to derive the restrictions on the lens resolution.

Let us make use of the half-intensity criterion. Let the image of two point sources separated by the distance δ be resolvable when the transmission coefficient lies in the range of $[1/\sqrt{2}, \sqrt{2}]$. The critical value of $k_y^{\max}$, for which this condition is still valid, equals π/δ. Such a criterion of resolution power is stronger than the Rayleigh criterion, since it not only provides the given resolution but also ensures image reconstruction with minimal distortions. The half-intensity criterion competes with another fundamental resolution limit derived in Ref. [70] grounded on the structure periodicity of superlenses based on media consisting of wires.

Here, it is of primary importance to note that a small variation in frequency can substantially change the resolution of the device. For example, for fixed wire medium parameters [58], $kd/\pi = 0.996$ corresponds to a resolution of $\lambda/34$, and for $kd/\pi = 0.96$, the resolution falls to $\lambda/10$ (d being the lens thickness). In fact, this means that the frequency band in which it is possible to get resolutions no worse than $\lambda/10$ amounts to only 4%. In Ref. [56], a subwavelength resolution was achieved for 18% of the bandwidth.

A few words should be said about the material for a nanowire medium for operating at optical frequencies. At frequencies higher than 30 THz, the absolute value of silver permittivity is not high enough to realize the canalization mode [71], and silver should be replaced with gold or aluminum.

The first experiment in which superresolution was obtained using a wire medium in the near IR range was demonstrated in Ref. [64]. Gold rods 12 nm in diameter and 10 μm long were melted into an aluminum matrix. The distance between the rods was about 50 nm (Fig. 10). The authors of the paper managed to fabricate a structure of rods with such a thickness in a matrix more than 10 mm in diameter, keeping the rods from crossing each other. The superlens provides a resolution at a level of $\lambda/4$ in the wavelength range from 1510 to 1580 nm.

In recent years, a number of papers have been published developing the idea of superlenses on media consisting of wires. Thus, the authors of Ref. [72] propose an original solution for creating a material of wires and graphene sheets for imaging in the terahertz range. The near-field transmission of images at THz frequencies can be of importance in such applications as the detection and measurement of the mass and volume of small-scale biological substances (e.g., blood cells), many organic molecules, radioactive atoms, microbes, viruses, and particles of explosives. In the structure of Ref. [72], plasmonic modes excited in graphene interact with the propagating modes inside wires. Due to this interaction, it was possible to achieve a resolution of the order of $\lambda/10$ in a wide frequency range of 5–65 THz. Moreover, a possibility was demonstrated of controlling the metalens properties by changing the graphene chemical potential. Although Ref. [72] presents detailed instructions on the possible experiment, no experiment itself has been performed with such a structure.

As a curios issue, we note that, in the literature, the three-dimensional structure of metallic nanorods, proposed by the team of S Kawata [73] for subwavelength imaging in the short-wave visible region, is often not distinguished from a medium consisting of nanowires. In fact, such a structure is different from a wire medium. It is a resonant superlens that uses for transmitting near-field images the localized surface plasmons arising in the nanorods, which are strongly coupled to each other electrodynamically by locally enhanced near fields.

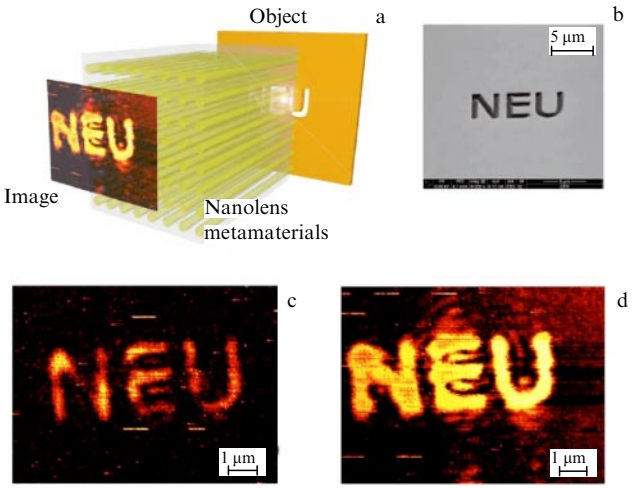

Figure 10. (Color online.) (a) Subwavelength resolution imaging with a superlens based on a wire medium at a wavelength of 1550 nm. Superlens consists of metallic wires placed in a dielectric. Such a metamaterial allows transferring subwavelength details of the image source over considerable distances, exceeding the wavelength (λ) by more than six times. (b) Image of characters NEU cut in a gold metal film 100 nm thick obtained using a scanning electron microscope (SEM). Character width is 600 nm (0.4λ) (c) Scanning the image source in the near field at a wavelength of 1550 nm by means of a scanning near-field microscope (SNOM). (d) SNOM scanning of the image obtained by means of a superlens located above its surface [64]. (Figure from Ref. [64] reproduced courtesy of the American Institute of Physics; permission received via the Copyright Clearance Center, Inc.)

The physics of such superlenses is considered in Ref. [65], where their drawbacks are also discussed in nearly the same way as those of the Pendry lens. Compared to a continuous layer of silver, the nanorod superlens has only one, albeit an important, advantage — the possibility of operating at several frequencies. However, the relative frequency range of a canalizing superlens in the near-IR region turns out to be wider, and, therefore, the practical advantage of the Kawata superlens is only the short-wavelength range of optical frequencies at which it can operate, in contrast to the canalizing superlens.

The authors of Ref. [73] proposed using a structure consisting of metallic nanorods to transmit images of incoherent sources; it was also shown in [74, 75] that it can be applied for working with coherent sources as well.

Cascading the structures of metallic nanorods with small gaps between the arrays [76] can provide the transmission of images with subwavelength resolution in a wide frequency range (up to transmitting color images), but only for an incoherent source. In the case of coherent sources, the functioning of such lenses is restricted to a narrow frequency range [77], whose relative width is nearly equal (a bit smaller than) that of the canalization.

3.2 Canalization of near-field images in a one-dimensional metamaterial and resonant tunneling in a photonic crystal

Although it is exactly wires (nanowires in the IR range, microwires in the THz range) that are most frequently used to canalize near-field images, this is not necessary. As shown in Ref. [57], canalization is also possible in a periodic structure of alternating silver and dielectric nanolayers, where, upon the appropriate choice of layer thicknesses (the thickness of silver nanolayers should be much less than the skin layer thickness), quasi-planar isofrequency surfaces appear in the long-wave part of the visible range. Simultaneously and independently, this result was obtained in Ref. [78].

Based on calculations, the authors of Ref. [79] compare the properties of similar nanostructures with various dielectrics: SiO, SiO_2, SiC, Si_3N_4, Si. The results of modeling the formation of images of fluorescent markers using a metalens of N layers of metal and $N+1$ layers of dielectric ($N \leqslant 5$) were demonstrated. The model used also takes into account the change in the emission rate of a fluorescent marker because of the environment's inhomogeneity. Tuning the metalens parameters and the distance from the object to the lens, the authors of Ref. [79] show that a regime exists in which plasmon amplification at the metal–dielectric interface together with the transmission effects lead to a very impressive subwavelength resolution. For $N = 5$, the distance between two markers that can be theoretically resolved in visible light is $\Delta = 5$ nm (of the order of 0.01λ) for point objects separated from the lens by a distance of up to 30 nm.

The internal period of the canalizing structure is much less than the wavelength, not only in the free space but also in the dielectric medium separating the silver layers. Therefore, this structure is a one-dimensional metamaterial, i.e., an effectively continuous resonant medium. Unfortunately, the subwavelength resolution in such structures turns out to be too sensitive to the geometric parameters of the layers, and in the course of practical implementation, deviations in the layer thickness are technologically unavoidable; the distortions of fields from different layers in such a superlens sum up and eliminate its subwavelength resolution already at $N > 2$ [80, 81].

However, the regime of near-field image transmission close to the canalization regime is observed not only in extremely anisotropic continuous media but also in some photonic crystals. In Ref. [81], this mode was called the resonant tunneling of an image. At first, this mode was obtained as a numerical result without explanation in Refs [70, 82–85]. Then, in Ref. [54], an analogy was revealed between the transfer of near-field images through a photonic crystal layer and the canalization mode. Indeed, in spite of the presence of inclusions comparable in size to the wavelength, a number of photonic crystals have extremely high anisotropy, which relates them to continuous extremely anisotropic materials. In such photonic crystals, the isofrequency surfaces can be approximately planar, which explains the resonance tunneling.

The short paper [86] published in 2003 could be considered the first experimentally confirmed result on subwavelength resolution. The image was formed at a distance of 2.75 cm from the back surface of the lens in a narrow frequency range from 9 to 9.4 GHz with the best focus at a frequency of 9.3 GHz (Fig. 11).

However, in contrast to media consisting of wires, photonic crystals cannot be homogenized; therefore, it is more difficult to use them for subwavelength imaging. An evanescent wave (as well as a propagating one) upon incidence on a photonic crystal layer with a planar isofrequency surface creates, in addition to a wave propagating across the layer, a few evanescent waves, which affects the amplitude and phase of the transmission coefficient. As a result, the transmission coefficients for different spatial frequencies turn out to be substantially different, and this difference does not decrease upon variations in the layer thickness. Therefore, it turns out to be impossible to formulate theoretically the sufficient conditions for optimizing such a superlens. Numerical studies are necessary.

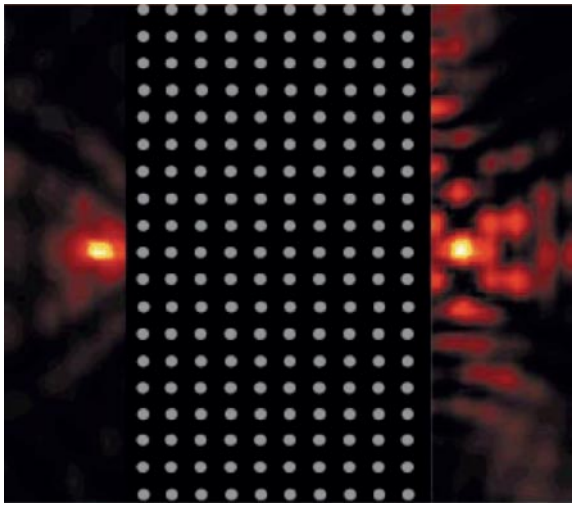

Figure 11. (Color online.) Two-dimensional map of electromagnetic field intensity in the system 'source (left)–plane lens–image (right)' [86]. Geometric dimensions of the map are 37.5×30.0 cm. Source intensity varies from -20 dB (yellow) to -48 dB (black); intensity of the image from -30 dB to -75 dB. (Figure from Ref. [86] reproduced courtesy of © Springer Nature 2003.)

In 2003, the team headed by C Soukoulis (who, as far as we know, was not aware of paper [37] by Silin) numerically and experimentally obtained both the mode of all-angle negative refraction and a pseudoscopic image in a photonic crystal layer with a circular isofrequency [47, 48]. At the same time, the team also obtained subwavelength resolution of two microwave sources in a layer of a photonic crystal of dielectric cylinders in air [88] (it was later shown that in this case the isofrequency surface of the photonic crystal is nearly planar). The effective width of the image of a practically point source amounted to 0.21λ in the measurements [88]. Two years later, paper [89] was published, in which a two-dimensional image was obtained using a three-dimensional photonic crystal. The half-width of the image maximum repeated that of the source and amounted to 0.35λ. In 2009, an experiment with a one-dimensional photonic crystal consisting of layers of aluminum oxide separated by layers of an optically less dense dielectric [90] demonstrated a spatial resolution of 0.27λ in the microwave range.

The first attempt to get a subwavelength resolution in photonic crystals operating in the optical range, namely, in the near-IR range, is related to 2006. In Ref. [91], a layer of two-dimensional photonic crystal was a lattice of round holes with a micrometer period in a silicon film 260 nm thick on a glass substrate. The attempt was unsuccessful: because of overlap of aberrations and the subwavelength image, the effective width of the point source image turned out to be larger than a wavelength. Two years later, the authors of Ref. [92] managed to reduce the image size using a photonic crystal of triangular holes in an InP/GaInAsP/InP heterostructure on an InP substrate. But this was still far from real subwavelength imaging. In Ref. [93], it was pointed out that the surface (Tamm) states of a photonic crystal can play the key role for the image size and even lead to the appearance of aberrations.

All these hampering factors are taken into account in Ref. [94], where subwavelength resolution in the resonant tunneling mode combined with the pseudoscopic mode is reported (in this case, no Tamm states arise at the crystal boundaries). The spatial resolution experimentally achieved in Ref. [94] in the near IR regions (at the wavelength of 1.5 μm) was $\Delta = 0.40\lambda$. Such a photonic crystal superlens is an analog of the Pendry wave superlens, i.e., a practical implementation of the idea of such a lens, but without the backward propagating waves and the increase in evanescent waves.

In Ref. [95], it is shown that the point source image width can be somewhat reduced by gradient change of the refractive index of the photonic crystal layer [94] near the interfaces. The effective width of the point image demonstrated in this paper by numerical modeling amounted to 0.37λ.

Thus, although photonic crystal layers allow producing a subwavelength image and even matching it with the wave image at the expense of using the resonant tunneling mode, at optical frequencies the spatial resolution improvement turns out to be so modest compared to that of a common immersion lens that it is hard to justify the increase in the device cost. Therefore, the authors of papers published in recent years propose using photonic crystal superlenses not only and not exactly for imaging but for the diagnostics of an object [96, 97] or for demultiplexing, i.e., spatial separation of waves having different wavelengths [98, 99].

3.3 Canalization of near-field images in a hyperbolic metamaterial

According to Fig. 9, metamaterials with hyperbolic isofrequencies implemented in the visible frequency range as periodic structures of plasmonic metal nanolayers (silver or gold), alternating with nanolayers of a dielectric, do not seem very promising from the point of view of superlens creation in comparison with media consisting of wires. Nevertheless, it turns out that, by varying parameters in such a material, it is possible to change the curvature of its hyperbolic isofrequency surface, so that some of the isofrequencies become almost flat. Exactly this was the effect used in papers [57, 78, 79] already discussed above. Various superlens options using hyperbolic metamaterials for various frequency ranges were proposed, e.g., in Refs [57, 66, 100, 101]. A radiofrequency experiment in 2010 showed that superlenses based on hyperbolic materials can reach the resolution $\Delta = \lambda/200$ [100].

The authors of Ref. [101], devoted to hyperbolic superlenses operating at frequencies near the boundary between IR and visible light, consider such small layer thicknesses (of the order of 5 nm) that they begin to exhibit quantum effects. Such a superlens provides a resolution of $\Delta \approx \lambda/14$ at the wavelength corresponding to all-angle negative refraction in the metamaterial layer. An important advantage of such a wave (Pendry-type) superlens over a photonic crystal wave superlens is the possibility of controlling the negative refraction band by applying external voltage and changing the properties of quantum wells from which the lens is composed.

Improving superlens properties is possible by using an additional plasmon injection scheme of loss compensation. The introduction of an additional source allows reconstructing the weakened spectral components of the image with minor amplification of noise. The authors of Ref. [102] confirm their idea by the example of a lens made of hyperbolic metamaterials.

3.4 Hyperlenses

Hyperbolic metamaterials utilizing isofrequencies that are close enough to planar ones appeared promising for creating magnifying superlenses — hyperlenses.

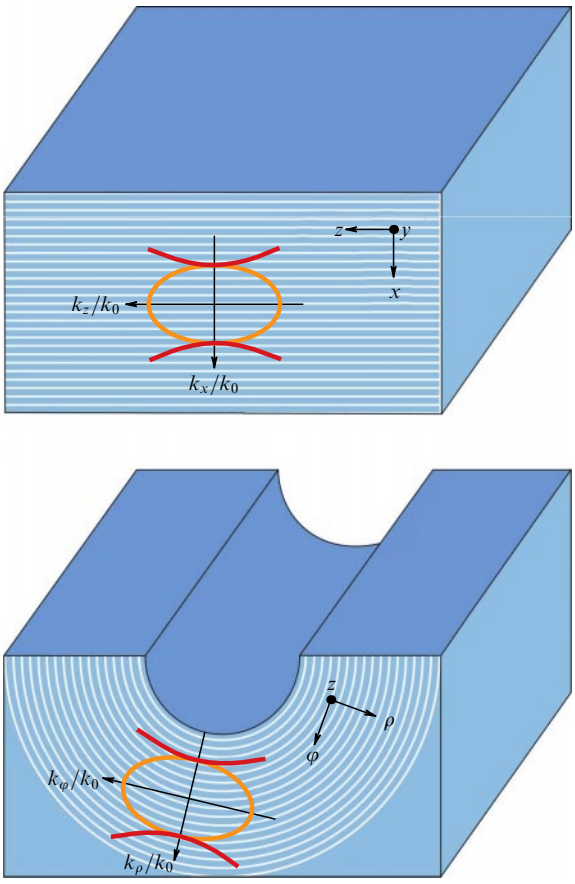

Figure 12. (Color online.) Anisotropic multilayer metamaterial in (a) rectangular and (b) cylindrical geometry. In the case of a curved metamaterial sample (b), the tangential component of the wave vector decreases as the wave propagates along the radial direction, as a result of which on the outer side of the metamaterial structure a magnified image is formed.

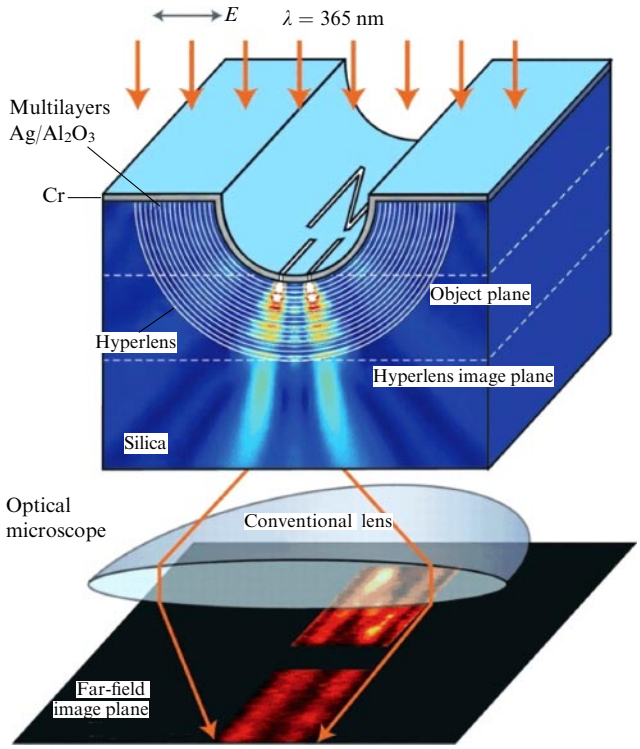

Figure 13. (Color online.) Schematic of a hyperlens and numerical modeling of images of subdiffraction objects [106]. (Figure from Ref. [106] reproduced courtesy of the American Association for the Advancement of Science; permission received via the Copyright Clearance Center, Inc.)

In a hyperlens, the spatial spectrum is compressed so that the incident evanescent waves that become propagating in the metamaterial reduce their spatial frequency (i.e., the transverse component of the wave vector) in the process of propagation. As a result, when reaching the back surface of the hyperlens, these waves do not convert into evanescent ones, but remain propagating. At the same time, the subwavelength information contained in them is preserved, because the reduction in spatial frequencies occurs uniformly all over the spatial spectrum.

In fact, the issue is a controlled (nondiffractive) divergence of the wave beam carrying the near-field image in the course of transmission. This effect is achieved by uniform bending of the hyperbolic metamaterial layer such that its initially planar boundaries become spherical (three-dimensional option) or cylindrical (two-dimensional option). Correspondingly, all nanolayers making up the metamaterial also become bent, as shown in Fig. 12. Thanks to the conservation of angular momentum $m = k_\varphi r$, the tangential components of the wave vector k_φ decrease as the wave propagates along the radial direction. The image magnification in this case equals the ratio of radii at two boundaries of the lens.

Such magnifying superlenses allow obtaining field distributions with subwavelength detailing at scales larger than the wavelength, which makes it possible to process them using the usual means of diffraction optics (Fig. 13) [35, 103]. Many research teams [104–107] have presented practical implementations of hyperlenses based on layered media.

To avoid the problem of absorption in materials and, thus, avoid image distortions in the far field, the hyperlens design should ensure that all rays from the object plane travel the same path length through the metamaterial. Scattering on the hyperlens surfaces can play the key role for visualization applications. Therefore, the hyperlens design should also ensure impedance matching between the lens and the environment [108, 109].

Other research teams have presented alternative solutions for magnifying subwavelength images, also related to conversion to curvilinear coordinates [110–113]. It has been shown that a transformation of wave vectors, similar to that occurring in curved layered metamaterials, can be achieved at the expense of unique dispersion curves of hyperlens materials, its external geometry remaining planar [111, 112, 114]; this is of particular importance for biomedical studies.

The first cylindrical hyperlens was practically implemented by depositing silver and aluminum oxide layers on the surface of a semicylindrical cavity in silica [115]. The hyperlens operated in the UV range of wavelengths and provided the resolution $\Delta \approx \lambda/3$ and twofold image magnification.

In Ref. [116], a spherical hyperlens was experimentally studied providing a resolution of 160 nm at a wavelength of 410 nm and image magnification by nearly 2.1 times. Silver nanolayers in a semispherical cavity formed the hyperlens. In Ref. [109], it was shown that the subwavelength resolution of a hyperlens can be improved by optimizing the ratio of thicknesses of plasmonic and dielectric material layers; also

proposed was a technology of fabricating so-called rolled-up hyperlenses subsequently developed in Refs [117, 118]. In Ref. [119], hyperlenses based on texturized layers were optimized, which made it possible to reduce the losses and to achieve higher energy efficiency keeping the image scale subwavelength.

Reference [80] discusses technical limitations of hyperlenses comprising metal/dielectric nanolayers. It is shown that, because of strong compensation of contributions from symmetric and antisymmetric eigenmodes excited in the lens material, its resolution reduces with an increase in the number of metallic layers. The authors point out that the optimal number of metal layers cannot exceed 20. Moreover, they studied and explained the effect of losses in the metal, granularity, and the volume fraction of metal on the image quality. Their main conclusion is that multilayer metal-dielectric hyperlenses do not provide such a resolution and magnification that could justify the cost of their fabrication and, therefore, have no prospects of mass application. They can find use, possibly, only in particular applications of near-field microscopy, when it is necessary to increase the distance between the object and the image.

Reference [120] proposes that the excitation of hyperbolic phonon polaritons at the interfaces of a plane-parallel boron nitride plate be used to get superresolution without image magnification. Such a structure is a full analog of the silver Pendry superlens, because, due to the presence of coupled surface states, the growth of evanescent waves in the direction from the source occurs in it. On the other hand, it can be classified as being a hyperlens, since its material is optically transparent and has a hyperbolic dispersion in the operating range of frequencies, i.e. in the far IR range.

Such a hyperbolic Pendry superlens has much better resolution than a silver one. Its theoretical spatial resolution at the optimal thickness is $\Delta = \lambda/40$, and, in the experiment, it turns out to be $\lambda/32$. In spite of such record-breaking resolution, the application of this superlens for imaging subwavelength details *in vivo* is not relevant, since the actual wavelength is 12 μm. Such superlenses, according to [120], can find application in photonic computing or become the basis for an ultracompact subwavelength spectrometer.

3.5 Endoscopes with subwavelength resolution

By replacing the hyperbolic metamaterial with a wire medium, it is possible to obtain a superlens, in which the length of the wires is much greater than its transverse size. If, in addition, these wires are made to diverge uniformly over the sample cross section, then, in addition to canalization of near-field images, we will get their magnification. Simulations show that, if the angle between the edge wires and the axis of such a structure (endoscope) is not too large, the canalization mode will not be destroyed, and the magnification will depend on the slope angle of the wires and the endoscope length. It is interesting that the same endoscope can be used for both magnification and demagnification of the image, depending on the lens orientation with respect to the object.

Numerical modelling of a microwave superlens 1 m long with threefold image magnification was carried out in Ref. [121]; at the same time, in Ref. [62], a fivefold magnification is reported. In experimental samples, operating in the microwave range [100, 122], it was possible to achieve a resolution of $\lambda/30$ with a threefold image magnification. However, in the microwave region, such structures find no application. Subwavelength resolution endoscopes with image magnification are in demand in the THz range [62, 123, 124], as well as at the megahertz frequencies used in magnetic resonance tomography (MRT) [125, 126].

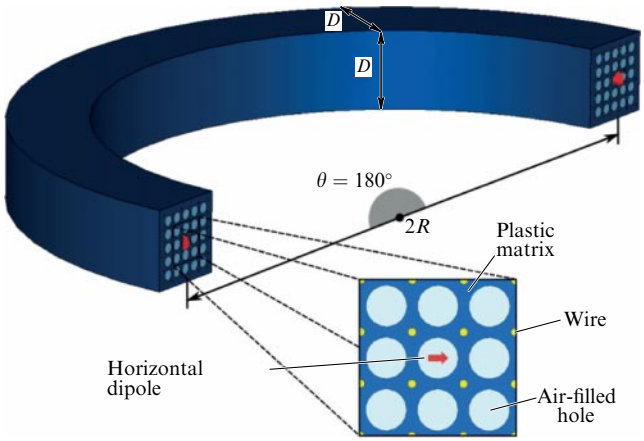

Figure 14. (Color online.) Flexible terahertz endoscope with an array of 6×6 wires in a polymer matrix [127]. (Figure from Ref. [127] reproduced courtesy of © The Optical Society.)

In Ref. [127], the properties of a terahertz endoscope based on metallic microwires were analyzed for various bending angles (Fig. 14). It turns out that bending of the waveguide affects its transmission frequency bands. The microwave range experiment confirmed this harmful effect predicted by simulation. Even a slight bending of a waveguide leads to a change from the 'maximum power transmission, minimum losses' state to the 'minimum transmission, maximum losses' state at a fixed frequency. In this situation, the subwavelength resolution no longer makes sense, since the primary optical signal does not reach through the endoscope even in the forward direction from the source to the object. The data obtained show that the use of terahertz endoscopes, in which subwavelength resolution is provided by a wire medium, is associated with significant difficulties.

At megahertz frequencies in MRT, this effect has no significance, because, as a rule, no endoscope bending occurs in this case. Moreover, the length of endoscopes used in MRT is not a hundred wavelengths as in a terahertz endoscope, but exactly half a wavelength. Therefore, even upon bending, the coefficient of power transmission through the endoscope at its operating frequency decreases insignificantly.

4. Metalenses with subwavelength focusing and subwavelength resolution based on metasurfaces

Simultaneously with the development of superlenses based on three-dimensional materials, development of the metamaterials concept proceeded towards simplifications. Probably, the most practically important simplification is the replacement of a bulk metamaterial with a surface one. In this case, the term 'metamaterial' is preserved for a bulk medium with artificial inclusions (either resonant or providing an unusual frequency or spatial dispersion), while an optically thin array of inclusions of this kind is referred to as a metasurface [6, 128].

The frequency of mentions of the term 'metamaterial' in the English-language literature rapidly grew in the early 2000s, which slowed down by the early 2010s and finally gave way to a decline in recent years. Simultaneously, mentions of 'metasurface' as a two-dimensional analog of a

bulk metamaterial became more and more frequent. From 2015 to the present day, the frequency of using this term is in the zone of nonlinear growth. This is not surprising, since metasurface properties depend on the mutual arrangement of inclusion only in two dimensions, instead of three as in metamaterials.

Fabricating a bulk nanostructured metamaterial for operating in the visible range of frequencies is a task at the limit of modern technological capabilities, whereas metasurfaces can be produced using standard methods, among which the most expensive and slow is electron lithography. There are a number of available and inexpensive technologies based on the self-organization phenomenon.

The key question for our review is whether a metalens obtained by removing one dimension in a metamaterial could provide subwavelength focusing and subwavelength resolution. The answer to this question is affirmative.

Metasurfaces can locally change the phase of a transmitted or reflected wave, which is thoroughly considered in review [6]. This property offers a possibility of light focusing by an azimuthally symmetric metasurface with radially nonuniform density and orientation of meta-atoms (inclusions).

Let us briefly recall what kind of metalenses were discussed in Ref. [6]. Controlling the size and/or orientation of inclusions (meta-atoms), it is possible to achieve a hyperbolic profile of the phase shift in the radial direction. When the lens is illuminated by a plane wave, such a phase distribution ensures the transformation of the plane wave front into a spherical one converging on a point [129]. Metalenses designed in this way possess a number of advantages compared to refracting lenses, such as the planarity of technology, subwavelength thickness, the absence of spherical aberrations, and many others [130]. However, the light focused in this way is concentrated at a distance from the metalens comparable to a wavelength, and the converging wave beam obeys the same Abbe diffraction laws as in the case of conventional lenses. Therefore, the spatial resolution of such lenses is limited by the Rayleigh criterion.

The above limitation can be overcome with metasurfaces using other physical mechanisms. The following methods of subwavelength focusing and subwavelength resolution are known: using two metasurfaces parallel to each other, creating zone plates for evanescent waves, using phase conjugation of the wave front, and so-called superoscillations in the space domain. Moreover, by using frequency scanning and digital processing of the measurement data, it is possible to implement subwavelength resolution with only one resonant metasurface.

4.1 Superresolution using a double metasurface

In the simplified analytical model, the principle of operation of a superlens consisting of two metasurfaces strongly coupled by near fields is analogous to that of the Pendry lens. In Section 2, we mentioned that this physical mechanism has an analog in the theory of elastically coupled oscillators. Let us discuss it in more detail, following Ref. [131].

Let two similar pendulums be coupled by a spring (Fig. 15a). In the absence of the spring, each pendulum is an oscillator with a single resonance frequency ω_0. The spring couples the oscillators, and in the system the resonance is split into normal modes with oscillation frequencies $\omega_1 < \omega_0$ and $\omega_2 > \omega_0$. If an external force **F** drives the first pendulum at the individual resonance frequency ω_0, then the oscillation amplitude of the second pendulum turns out to be much larger than the oscillation amplitude of the first one. Moreover, for any frequency within the range $\omega_1 < \omega < \omega_2$, the oscillation amplitude of the second pendulum is greater than that of the first one, i.e., $\theta_2/\theta_1 > 1$, and this ratio reaches a maximum at frequency ω_0. (At frequencies ω_1 and ω_2 of the normal modes, the entire system behaves like a single oscillator and $\theta_1 = \pm\theta_2$).

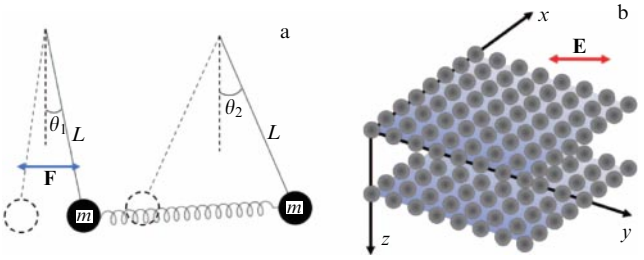

Figure 15. Illustration of the concept of coupled metasurfaces: (a) system of elastically coupled pendulums driven by oscillating external force **F**, (b) system of two plasmonic metasurfaces excited by a hot spot of light with electric field **E**. (Figure from Ref. [131] reproduced courtesy of © American Physical Society 2019.)

In the Pendry superlens, the role of the pendulums (Fig. 15b) is played by surface plasmon polaritons at the boundaries of the layer of the material with a negative real part of the complex permittivity. The dispersion curve of a single plasmon polariton in the region of evanescent waves $k_t > k_0$ is practically a horizontal straight line, so that for any k_t the interface is an oscillator with one and the same eigenfrequency. In the case of a layer with finite thickness, these oscillators are coupled by evanescent waves, which is equivalent to elastic coupling. The dispersion curve splits into two curves, both still close to horizontal straight lines at $k_t > k_0$. Thus, the amplitudes of all spatial harmonics of a plasmon polariton wave packet on the back surface will be greater than on the front one. Since all these surface waves are induced by incident evanescent waves, this effect means nothing but the exponential growth of evanescent waves across the superlens.

In Ref. [132], it is hypothesized that the surface waves (polaritons) at resonant metasurfaces, being dense lattices of resonant elements, behave in a similar way. In such a case, a pair of parallel metasurfaces separated by a small gap will possess the properties of a Pendry superlens. Moreover, the Pendry superlens effect will be expressed much more strongly, because, in a layer of a metamaterial, the evanescent waves are indeed hybrid due to optical losses. At the same time, in the dielectric gap between the metasurfaces, purely evanescent waves are present. By using curved metasurfaces, it is possible to create magnifying superlenses [132].

These hypotheses were confirmed for microwave superlenses by a number of computational and experimental studies, in the course of which an enhancement of evanescent waves uniform over the spatial spectrum was demonstrated, subwavelength imaging and resolution were obtained, and superlens optimization was carried out with a deviation of dispersion curves from the horizontal in the region of surface waves taken into account [132–135].

Realization of this idea for the visible frequency range, where the resonant scatterers could be nanospheres of a plasmonic metal, was proposed in Ref. [136]. Then, in Ref. [137], calculations for two square lattices of silver nanospheres demonstrated the resolution of two point dipoles equal to $\Delta = 0.34\lambda$, the image being theoretically formed at a

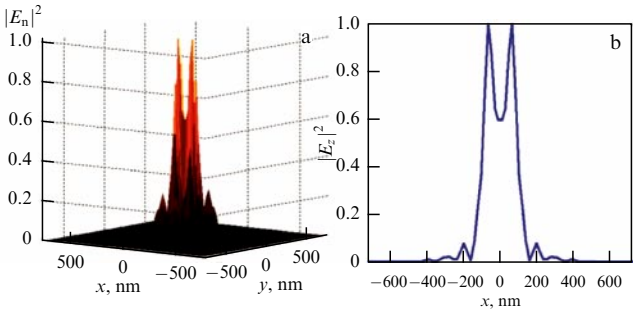

Figure 16. (Color online.) (a) Calculated electric field distribution in the image plane in the case of two vertically polarized sources. (b) Projection of the distribution in plane $y = 0$ [138]. (Figure from Ref. [138] reproduced courtesy of © American Physical Society.)

distance of $0.55\lambda = 240$ nm from the object, and the gap between metasurfaces was equal to 0.3λ. When nanospheres were replaced with nanospheroids, as was done in Ref. [138], the resolution could be improved only insignificantly (to 0.31λ) (Fig. 16), but the bandwidth within which the resolution of $\Delta < \lambda/2$ was achieved became extended to 13%.

In Ref. [131], it was shown that for a plasmon superlens the simplified model of a double metasurface is inadequate. The near-field interaction between the lattices of plasmonic spheres cardinally changes the shape of the split dispersion curves as compared to the dispersion curve shape of a single metasurface. Therefore, the optimization carried out for simplicity in Refs [137, 138] for one metasurface is not an optimization for a pair of them.

True optimization requires calculating dispersion for two coupled metasurfaces, for which in [131] an analytical model was constructed based on techniques recently developed to accelerate the convergence of dipole lattice sums. After optimization, it turned out that, for frequencies in the visible range, a square lattice of silver nanospheres with a diameter of $\lambda/8$ and period of $\lambda/6$ allows getting a resolution of two dielectric nanospheres at a level of $\Delta = \lambda/6$. In this case, the superlens thickness is nearly $\lambda/2$, and the distance between objects located on one side of the superlens and their images on the other side amounts to nearly 0.6λ. However, this is still only a theoretical result.

The disadvantage of such superlenses, which use lattices of resonant particles, is that their action extends only to evanescent waves. To focus the propagating part of the spatial spectrum, negative refraction is necessary, which is not implemented by regular linear metasurfaces. This disadvantage can be overcome using nonlinear metasurfaces. In Ref. [139], it is shown that a pair of parallel metasurfaces characterized by the phase-conjugate boundary conditions

$$\mathbf{E}_{t+} = \mathbf{E}_{t-}^{*}, \qquad \mathbf{H}_{t+} = \mathbf{H}_{t-}^{*} \tag{7}$$

operates as a perfect superlens. In the time domain, the complex conjugation of tangential components of the fields on both sides of the surface corresponds to time reversal.

Possible implementation based on lattices of nonlinear and nonreciprocal bianisotropic particles was proposed and analyzed in Ref. [140]. The most important feature of the proposed structure is its different response to propagating and evanescent waves. In the microwave region, the necessary properties can be realized using balanced modulators. In principle, in these nonlinear and nonreciprocal lattices, the amplification of evanescent modes also occurs due to resonance surface modes. Using phase conjugation has also been proposed in Ref. [141], but the metasurfaces described there should possess a nonrealistic efficiency as parametric amplifiers.

Returning to the concept of two coupled metasurfaces, we note that, for a perfect subwavelength resolution in such structures, it is desirable that the coupling between resonant elements in the lattice be minimal. Each particle would then be excited only by the incident field at the place of its location, which would ensure point-by-point formation of the image. Of course, it is impossible to eliminate coupling between the lattice elements, but this disadvantage can be turned into an advantage using the frequency scanning principle [142].

Consider a planar regular lattice of small resonant particles with the period substantially smaller that the wavelength. In the microwave range, this could be, for example, a lattice of small metallic spirals, or in optics, a lattice of silver nanospheres. Such a lattice of coupled resonators has many resonance modes — as many as the elements in the lattice. If the elements are coupled weakly, then the resonance frequencies are close to that of an individual inclusion.

Suppose that we know (from measurements or calculations) the spectrum of the lattice eigenmodes. If the lattice is excited by a plane wave (propagating or evanescent) at the frequency of one of the lattice modes, the amplitude and phase of oscillations of induced currents in the lattice will be determined by the amplitude and phase of the incident wave. In the superlens proposed in Ref. [142], the object under study is irradiated by a wave whose frequency changes within the resonance bandwidth of such a lattice, used as a sensor. The field scattered by the object is expanded in a spatial Fourier series, and the amplitudes and phases of the harmonics are determined by measuring the amplitude and phase of the field near two or three arbitrarily chosen lattice elements. The spatial distribution of the field is found by numerical summation of the Fourier series. It is interesting that the numerical summation can be avoided using two parallel lattices.

4.2 Superresolution using a zone plate for evanescent waves

The idea of overcoming the Abbe limit for resolution at a level of $\Delta = 0.5\lambda$ using a perforated silver nanolayer, which is a zone plate for evanescent waves, was first presented in Ref. [143], but was not implemented, even using calculations. R Merlin theoretically obtained subwavelength focusing in such a structure in 2007 [144].

Fresnel-type zone plates for evanescent waves implement the principle of nonradiative interference. This interference redistribution of evanescent waves in space leads in this case to a substantial increase in the electric field amplitude on the axis of the plate. As a rule, evanescent fields are not associated with phases, like propagating waves; however, in the plane perpendicular to the axis along which the evanescent wave decays, it is propagating and has a phase front, which makes nonradiative interference possible.

For simplicity, consider a subwavelength zone plate in the case of cylindrical symmetry. Then, instead of a point, the ideal focus is a straight line parallel to the y-axis, and any component F of the electromagnetic field obeying the Helmholtz equation can be expressed as

$$F(y, z_\alpha) = \frac{1}{2\pi} \int \int_{-\infty}^{+\infty} F(y', z_\beta) \exp\left[\mathrm{i}q(y - y') + \mathrm{i}\kappa(z_\alpha - z_\beta)\right] \mathrm{d}y' \, \mathrm{d}q, \tag{8}$$

where

$$\kappa = \begin{cases} \mathrm{i}\left|\left(q^2 - \dfrac{4\pi^2}{\lambda^2}\right)^{1/2}\right|, & q > k_0\,, \\ \left|\left(\dfrac{4\pi^2}{\lambda^2} - q^2\right)^{1/2}\right|, & q < k_0\,. \end{cases} \tag{9}$$

Equation (8) relates the values of field F on two planes: $z = z_\alpha > 0$ and $z = z_\beta > 0$. Let us set $F(y,0) = M(y)\exp(\mathrm{i}q_0 y)$; according to the data, $|q_0| \gg k$, i.e., the incident wave is evanescent with a large spatial frequency. Function $M(y)$ is determined by the local transmission coefficient of the plate, located in the plane $z = 0$. Let us find $F(y,z)$ using Eqn (8) and approximating $\kappa(q) \approx \mathrm{i}|q_0|$:

$$F(y,z) \approx \frac{1}{2\pi}\int\int \exp(\mathrm{i}qy)\exp(-|q|z)M(y') \times \exp\left[\mathrm{i}(q_0 - q)y'\right]\mathrm{d}y'\,\mathrm{d}q\,. \tag{10}$$

A sufficient condition for evanescent wave focusing is the existence of a pole in the complex plane y. For example, the quite realisable transmission function $M(y) = (1 + y^2/L^2)^{-1}$ has poles $y = \pm\mathrm{i}L$, field $F(y,L)$ at a distance $z = L$ from the plate being proportional to $L\exp(-q_0 L)|\sin[(q_0 y/2)/y]|$, as can be easily shown using Eqn (10). This corresponds to a subwavelength focal spot size, since $q_0 \gg k$.

This principle, confirmed by quantitative calculations (including three-dimensional ones) in Ref. [144], was further developed in Refs [145–148]. Numerical modelling [146] using the finite difference method in the time domain demonstrated that a metal-coated zone plate can provide subwavelength focusing for an evanescent wave in the visible range, the focal spot size being independent of the metal choice (silver, gold, aluminum, and tungsten were considered, the metal film thickness being 300 nm for all these metals). This result testifies to the fact that plasmon effects do not affect the phenomenon of subwavelength focusing, which, as in a conventional Fresnel zone plate, becomes possible exactly due to the low transparency of the metal nanolayer. Moreover, it was shown that the focus in the near field of an evanescent zone plate suppresses the higher-order foci, which increases the focusing efficiency.

Metalenses with corrugated surfaces were theoretically studied in Refs [149, 150]. The design of a metalens was described as consisting of a slit with a waveguide surrounded by linear nonperiodic grooves. It has been shown that aperiodic grooves can form a magnetic field profile in a focus with the effective width of $\lambda/15$ of the central maximum.

Since subwavelength focusing allows subwavelength resolution and the amplitude profile synthesis can be completed with the synthesis of the phase profile, a metalens based on evanescent zone plates can be used for subwavelength spatial resolution with magnification, like the plane-parallel hyperlens discussed in Section 3.4. This idea was realized in the microwave range. In Ref. [151], the metalens comprised an array of comb condensers printed on a thin substrate. The zone plate structure was optimized to provide image magnification by two orders of magnitude at the best resolution, approximately $\lambda/20$.

Note that the Fresnel zone plate for evanescent waves is a fundamentally nonperiodic metasurface. This gives rise to great difficulties in its experimental realization in the optical range, where it is a nanostructure. That is why there is no experimental data on this type of optical metalens.

The results for corrugated metalenses from Refs [149, 150] are experimentally confirmed in Ref. [152] also in the microwave range. The approach to superresolution, based on using thick metalenses, is experimentally checked in the microwave range [153], the best resolution being $\lambda/38$ at the physical distance of $\lambda/33$ between sources.

4.3 Superresolution via superoscillations

An important disadvantage of zone plates for evanescent waves is the strict limitation on the object position, the image of which is formed in the given plane. Indeed, since waves decaying along the z-axis are involved, the object should be separated from the zone plate by a distance much less than the wavelength, and this sets a hard limitation on possible applications of such metalenses.

Therefore, an alternative to zone plates was necessary — a metalens with similarly high spatial resolution, but allowing a farther location from the object, which would make it applicable for extended object imaging. The concept of so-called Aharonov–Pancharatnam–Berry superoscillations [154] became such an alternative. The idea of superoscillations in the time domain belongs to Y Aharonov [155, 156]. Later, M Berry [157] described the relation between Aharonov superoscillations and the concept, known as the Pancharatnam–Berry phase, which was formulated much earlier than Aharonov's idea and introduced in quantum electrodynamics.

The concept of superoscillations developed for the time domain has been adapted to the space domain, as shown in Refs [158–160]. In these papers, the relation of superoscillations to one more earlier known effect, the Schelkunov superdirectivity of antenna arrays, was revealed. The use of superoscillations for both temporal and spatial superresolution is thoroughly discussed in review [161].

Following Ref. [162], let us consider the concept of superoscillations before proceeding to their application in physical systems. A signal function is called superoscillating if the maximal frequency of the signal oscillation exceeds the maximal frequency of its frequency spectrum. How is this possible?

Consider a periodic function $f(x)$. If its Fourier spectrum

$$\tilde{f}(\omega) = \frac{1}{2\pi}\int_{-\infty}^{\infty} f(x)\exp(-\mathrm{i}\omega x)\,\mathrm{d}x \tag{11}$$

is zero beyond the frequency band $-\Omega < \omega < \Omega$, then it is commonly accepted that the function itself changes with a period of less than $2\pi/\Omega$. However, this is not necessarily so. For example, the function (see [155, 163])

$$f(x) = (\cos x + \mathrm{i}a\sin x)^N\,, \tag{12}$$

where $N \gg 1$ and $a > 1$ (sometimes referred to as the canonical superoscillating function) can be written in the Fourier representation with the maximum frequency of oscillations equal to N, which is due to appearance of the terms $\sin^N x$ and $\cos^N x$ when removing the brackets in Eqn (12). However, if we consider the asymptotic behavior of function $f(x)$ in the neighborhood of $x = 0$, then, after decomposing the oscillating harmonics into a Taylor series, it turns out that the maximal frequency at which the function oscillates equals aN. Indeed,

$$f(x) \approx (1 + \mathrm{i}ax)^N = \exp\left[N\log(1 + \mathrm{i}ax)\right] \approx \exp(\mathrm{i}aNx)\,. \tag{13}$$

Here, we made use of the Taylor expansion of the logarithmic function and took into account that x is small. Obviously, the oscillation frequency of the obtained function is aN. Note that the canonical superoscillating function is smooth, which allows analyzing its properties analytically. After simple mathematical operations, it can be presented as

$$f(x) = \left(\frac{a}{k(x)}\right)^{N/2} \exp\left(\mathrm{i}N\int_0^x k(x')\,\mathrm{d}x'\right), \tag{14}$$

where the wave number $k(x)$ is defined as

$$k(x) = \frac{a}{\cos^2 x + a^2 \sin^2 x}\,. \tag{15}$$

Figure 17 illustrates the behavior of the canonical superoscillating function at various argument scales. The fastest oscillations — superoscillations — occur near zero, where the local wave number is $k_{\max} = aN$ and the oscillation period is $\Delta x_{\min} = \pi/(aN)$ (Fig. 17a). The slowest oscillations correspond to the wave number $k_{\max} = N/a$, the distance between adjacent extrema being $\Delta x_{\max} = \pi a/N$ (Fig. 17b). The function amplitude in the region of slow oscillations is a^N times greater than in the region of superoscillations.

The last statement generalizes to any superoscillating functions. Superoscillations have their cost: the function amplitude between two closely spaced superoscillation zeros is much less than the maximal amplitude of the function. In Ref. [157], Berry made an attempt to answer the question of whether it is possible within a bandwidth of 1 Hz to obtain a signal reproducing the Ninth Symphony by Beethoven. Using superoscillations, it turns out to be possible; however, practical realization would require amplifying the signal 10^{19} times.

The extremely low amplitude of superoscillations makes them, at first glance, nothing more than an entertaining mathematical curiosity without practical application. However, this is not so, if we speak about applications where the superresolution is demanded.

The superoscillation concept was first realized in the space domain in 2007 [164, 165]. In spite of the low superoscillation amplitude, it was possible to record diffraction patterns from quasicrystalline arrays of nanoholes. In 2008, the same authors reported that a quasicrystalline array of nanoholes in a metallic screen can simulate pseudolens properties, forming an image of a source without magnification at a distance of a few ten wavelengths from the lens [166]. The measured spatial resolution of the lenses was comparable to the resolution of traditional lenses with a high numerical aperture, namely, at a wavelength of 660 nm the effective focal spot width was 360 nm.

N Zheludev's team presented the first design of a one-dimensional superresolution lens in 2009 [167]. To achieve superresolution, the distribution of fields in the lens focal plane should be a superoscillating function. The formation of such a distribution beyond the near field region is possible using diffraction by a lattice. However, for this purpose, it is necessary that the superoscillating function of field distribution in the focal plane be expanded in a spatial Fourier series, i.e., represented as a superposition of plane waves.

Therefore, a major step in the development of metalenses is the search for plane-wave decomposition of the transmitted field with a limited bandwidth of spatial frequencies. The wave functions of a prolate spheroid turn out to be a good candidate for this goal. It is important not only that

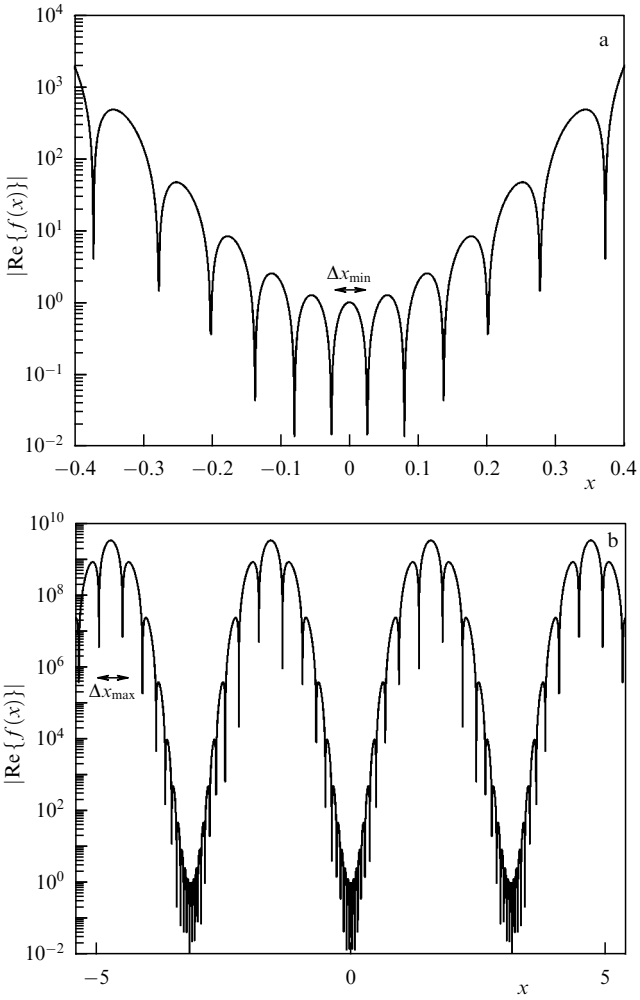

Figure 17. Canonical superoscillating function with parameters $a = 3$, $N = 20$ for argument values (a) $-0.4 \leqslant x \leqslant 0.4$ and (b) $-5.4 \leqslant x \leqslant 5.4$. (Figure adapted from Ref. [162].)

spheroidal wave functions form a complete set, but also that they be restricted to propagating waves $[-k_0, k_0]$ in spatial frequencies. To construct such a metalens, algorithm [159] is used based on the reciprocity principle and transition from sources distributed in space to sources distributed in spatial frequencies.

Reference [167] states that the transition from the one-dimensional case to the two-dimensional one is trivial. However, the actual creation of two-dimensional metalenses based on superoscillations requires further development of the approach and the use of evolution algorithms, as was shown in Ref. [168]. The authors of Ref. [168] predicted the effective width of 0.29λ for a focal spot located in the far zone. A ring whose intensity significantly exceeds that at the focal point surrounds the round spot in the form of an Airy disc. This addresses the main drawback of superoscillations: the small intensity of superoscillations compared to the side parasitic signal (halo). But even if we disregard the ring and calculate the lens resolution power by the size of the focal spot, the spatial resolution of such a lens would improve insignificantly, whereas the initial concept of superoscillations promised an arbitrarily small (subwavelength) size of the point object image.

In recent years, considerable progress has been achieved in this field: methods have been proposed to reduce the spot

size, to extend the frequency range, and to use polarization response to enhance spatial resolution [169]. In addition, in the general theory of superoscillation, some new effects have been found [154]. In Ref. [170], it is shown that the problem of designing a superoscillating metalens can be solved as an inverse problem rather than as an optimization problem. This can substantially simplify the algorithm of finding optimal lens configurations.

In applications, to obtain optical images, the side parasitic signal is removed by means of confocal microscopy [160]. The formation of a superoscillation focus (hot point) is provided using a spatial light modulator, which allows changing its shape. Such hybrid microscopy offers better spatial resolution than does standard confocal optical microscopy. In addition, it allows the polarization contrast visualization of transparent objects (e.g., biological cells).

In Ref. [171], a polarization contrast microscope is developed for visualizing living nonmarked biological cells with spatial resolution, significantly exceeding that of the same microscope with standard illumination. Thus, the new technology of optical visualization allows nonalgorithmic visualization of nonmarked biological objects with superhigh resolution.

Another achievement in the field of creating superoscillation images is the development of a compact and cheap superoscillation lens, based on phase modulation masks. Such masks will allow achieving much more energy efficient hot points, in contrast to zone plates that control either the intensity or phase profile of the wave front by a binary method. However, at present, there is no technology for fabricating such masks. The situation is also complicated by the fact that there is no computation algorithm to reconstruct the image.

Recently a fundamentally new type of metamaterial was demonstrated — a 'superlens', which is a planar array of discrete subwavelength meta-molecules with individual scattering characteristics. The superlenses create superoscillating foci with arbitrary shape and size [172]. The new principle of a superlens made of a far-field metamaterial is demonstrated by manufacturing lenses and determining their characteristics in free space with previously inaccessible numerical apertures of up to 1.52 and the size of focal spots to 0.33λ. Such an approach opens new possibilities for upgrading commercial confocal microscopes by equipping them with superoscillation lenses that remove the limitation $\mathrm{NA} < 1$. Recent achievements have shown that this technology is realisable, but further work is needed to create efficient achromatic lenses with high transmission capacity, which will become an inexpensive replacement for conventional lenses. Superoscillation visualization is rapidly developing and at present is a field of primary importance in optical microscopy with subwavelength spatial resolution.

An example of an achromatic superoscillation metalens is presented in Ref. [173]. To be more precise, two variants of the metalens are proposed made of plasmonic (for the IR range) and dielectric (for the visible range) materials. Both metalenses have shown the spatial resolution characteristic of conventional immersion lenses without aberrations (of the order of 0.4λ). The authors of Ref. [174] managed to overcome the property of the subwavelength superoscillation focus to be surrounded by a high-intensity ring. The numerical simulation showed a focal spot size of 0.38λ without high-intensity neighboring zones with the radius greater than the wavelength. Such a result became possible

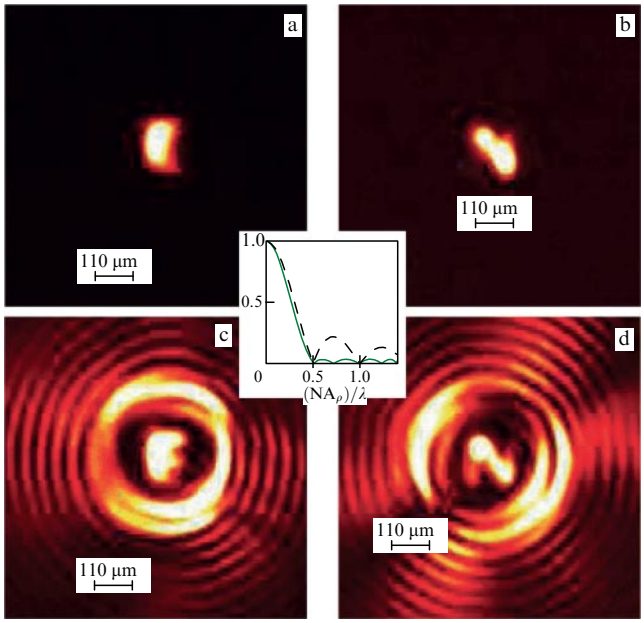

Figure 18. (Color online.) Experimental images of characters E and N with dimensions of 120×130 μm. Numerical aperture of the entire system amounts to 0.00864. (a, b) Images obtained using a traditional lens with the given numerical aperture. (c, d) Images obtained using a superoscillation metalens. Comparison shows that the characters are read much more clearly in the cases corresponding to the superoscillation lens. Inset in the center of the figure demonstrates the idea of the effect: although the main peak remains unchanged and diffraction limited, the intensity of next-order peaks can be substantially reduced at the expense of superoscillations, which leads to an improvement in image quality [175]. (Figure from Ref. [175] reproduced courtesy of © The Optical Society.)

by using the concept of selective superoscillations. Since electromagnetic waves obey the superposition principle, the field of a wave passed through a metalens can constitute a part corresponding to superoscillations in the focal plane and have no part that corresponds to the zone of high intensity around the focus. Reference [174] became an important step towards the practical application of superoscillations in nanophotonics.

In Ref. [175], an original idea was used to organize superoscillations not at the focal point but in its nearest neighborhood. By suppressing the signal near the focus (in turn, restricted by the diffraction limit), it is possible to substantially improve the resolution power of the system, which is confirmed by the experimentally obtained images in the visible range (Fig. 18).

Recently, results on superresolution of optical systems based on superoscillations have been qualitatively improved, and the resolution reached the value of $\lambda/20$. This became possible by using advanced methods of optimization, e.g., evolution algorithms. Thus, in Ref. [176], using a genetic *gamult* algorithm, optimization with respect to three target functions was performed. The focal spot width was minimized, as was the ratio of the field maximum outside the observation zone to the field at the focal point; in addition, the field maximum was minimized beyond the focal point, but within the zone of observation, which allowed removing the high-intensity zones near the focus. The optimization results show a resolution up to $\lambda/20$; however, the authors noted that at such a resolution the field amplitude in the focus is negligibly small, which means such systems have no prospects from the point of view of imaging. Nevertheless, the

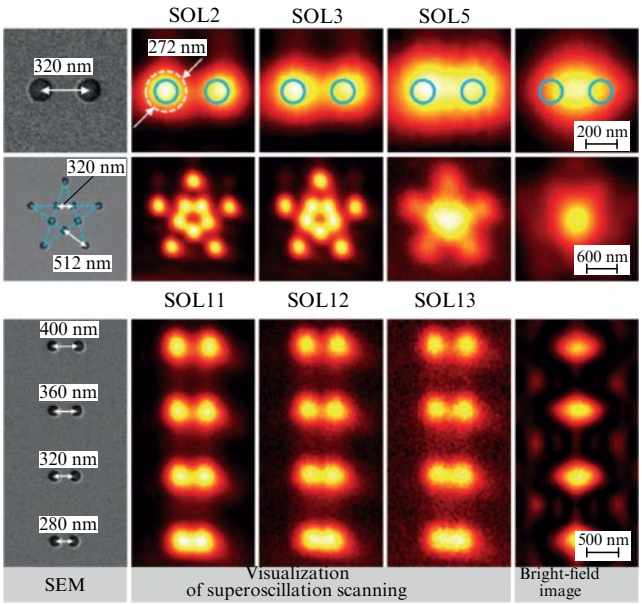

Figure 19. (Color online.) Images obtained using a superlens at a wavelength of $\lambda = 800$ nm. First column demonstrates SEM images of test samples: two holes 160 nm in diameter separated by a distance of 320 nm (0.4λ); ten holes of the same diameter separated by different distances from each other. Next three columns correspond to three different superoscillation lenses with a similar diameter of the observation zone equal to (λ) and different diameters of the focal spot: (0.33λ) (SOL2), (0.39λ) (SOL3), (0.56λ) (SOL5), as well as with a focal spot diameter equal to (0.39λ) and different diameters of the observation zone: (2λ) (SOL11), (4λ) (SOL12), (6λ) (SOL13). Last column refers to images obtained using traditional lenses with the same aperture [177]. (Figure from Ref. [177] reproduced courtesy of © American Physical Society 2019.)

authors recommend their method for systems with a resolution of about $\lambda/4$, in which the amplitude of the fields in the center of the focus is high enough.

In 2019, article [177] was published, which, despite its title, "Far-field superoscillatory metamaterial superlens," was exactly about a metasurface operating like a superoscillatory metalens rather than about conventional metamaterial superlenses. The metalens efficiently changes the transmitted wave local amplitude and phase due to figured holes in a gold film 100 nm thick on a silver substrate. In the mathematical description of superoscillations, the wave functions of a prolate spheroid were used. The experimental spatial resolution was $\Delta x = 0.28\lambda$. The results of the experiment are demonstrated in Fig. 19.

To finalize this section, we briefly mention the polarization transformation in metalenses with superoscillations. For usual metalenses, the polarization transformation problem was investigated in the papers by F Capasso's team (see, e.g., [178, 179]). It turns out that this function is possible in superresolving metalenses too. Thus, in Ref. [180], the possibility of transforming left-hand circular polarization into a right-hand one and vice versa using a superoscillation metalens is shown. However, the higher the metalens resolution power, the smaller the view angle. Therefore, metalenses with spatial superresolution require near-field scanning, which reduces the value of polarization transformation in them. Nevertheless, in Ref. [181], the possibility of using information on polarization in superoscillatory materials to improve the accuracy of diagnostics in some biological studies is pointed out.

5. Metalenses with subwavelength resolution based on turbid media

Light scattering in disordered (turbid) media (the Tindal effect) is an important tool for access to high spatial frequencies of the object studied. In contrast to the superoscillation method considered in Section 4.3, approaches based on turbid media allow forming an optical image in real time. As a result of multiple elastic scattering, near optical fields are generated in a turbid medium, the transfer of which to the far field provides a subdiffraction resolution. In practice, this is achieved using a defocusing near-field lens (or superlens) consisting of randomly spread nanoparticles (ZnO, TiO_2, GaAs, etc.) [182–185] or a rough surface of a plane-parallel plate of gallium phosphate [186]. A disadvantage of such a lens is the necessity of placing the studied object at a distance shorter than the wavelength of light.

In Ref. [185], a concept of a scattering diffusor lens separated from the object by a distance of 0.5 mm was proposed. A subwavelength resolution is achieved by reconstructing the wave front phase of the light scattered by an object using the ptychography method (a numerical algorithm of image reconstruction based on the processing of an array of two-dimensional interference patterns). The subwavelength optical visualization of objects can be implemented using the multiple inelastic scattering of light in a disordered nonlinear titanium oxynitride medium [51–53]. An enhancement of stimulated Raman scattering of light in a disordered nonlinear lens arises due to the excitation of plasmon resonance in a wide optical range. The considered class of superlenses provides a three- to five-fold advantage in spatial resolution.

Let us consider the physical mechanism of subwavelength spatial resolution due to multiple elastic scattering in a medium consisting of randomly spread nanoparticles, as schematically shown in Fig. 20a. An incident electromagnetic wave with the spatial vector k forms at the output of the defocusing lens a complex optical field with randomly oriented complex vectors $\mathbf{k}_m$ ($m = 1, 2, \ldots$). In the general case, the scattered field $\mathbf{E}_n$ comprises propagating and evanescent electromagnetic waves. The amplitudes $\mathbf{A}_m$ and phases φ_m of such waves are statistically independent random quantities. Since the elastic scattering is a linear process, the resulting field can be presented as

$$\mathbf{E}_n = \sum_m T_{nm}(\mathbf{k}_m)\mathbf{A}_m \exp\left(\mathrm{i}\varphi_m\right), \tag{16}$$

where $T_{nm}(\mathbf{k}_m)$ is the transfer matrix, containing the components of the optical near field. Although the incident electromagnetic wave does not contain imaginary wave vectors, in the near zone the scattered field (16) comprises such components. In the far zone, because of the random orientation of wave vectors, disordered speckles are formed whose dimensions are diffraction limited (Fig. 21a).

Visualization of the optical field in the near zone by means of scanning near-field optical microscopy (SNOM) demonstrates a significant reduction in the speckle size (Fig. 21b), direct experimental confirmation of the presence of imaginary wave vectors in the near zone. They allow forming a focal spot not limited by diffraction. For this purpose, the initial wave front of the incident radiation is divided into N channels with a spatial light modulator (SLM). Relative phases in each channel are detected by means of a SNOM probe, as shown in Fig. 20a. Then, the phases are controlled by the SLM, which

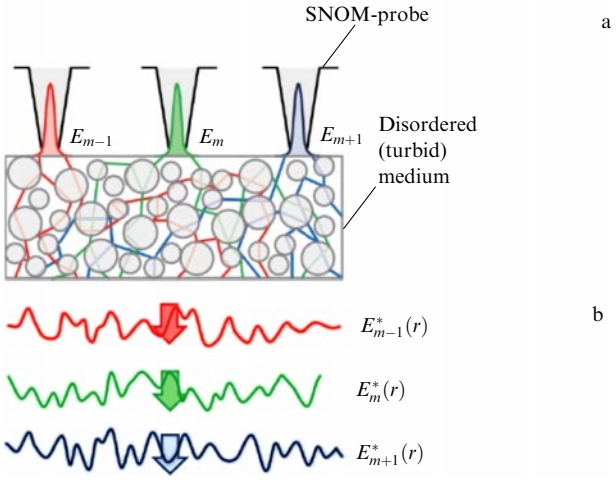

Figure 20. (Color online.) (a) Schematic illustration of an electromagnetic wave propagation from a point source, created by the subwavelength aperture of a SNOM probe, through a turbid medium. (b) Distributions of optical fields in the near zone from the corresponding point sources (shown in different colors) [182]. (Figure from Ref. [182] reproduced courtesy of © Americal Physical Society 2014.)

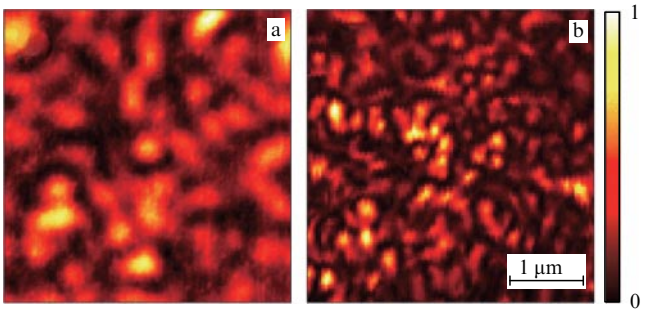

Figure 21. (Color online.) 2D optical image of a turbid medium in the far (a) and near (b) zones [183]. (Figure from Ref. [183] reproduced courtesy of © Springer Nature 2013.)

ensures constructive interference of the fields in the near zone and, correspondingly, subwavelength focusing. Using the recorded optical near fields, a transfer matrix is formed:

$$T_{nm} = \begin{pmatrix} \mathbf{E}_1(\mathbf{r}_1) & \mathbf{E}_2(\mathbf{r}_1) & \dots & \mathbf{E}_n(\mathbf{r}_1) \\ \mathbf{E}_1(\mathbf{r}_2) & \mathbf{E}_2(\mathbf{r}_2) & \dots & \mathbf{E}_n(\mathbf{r}_2) \\ \vdots & \vdots & & \vdots \\ \mathbf{E}_1(\mathbf{r}_m) & \mathbf{E}_2(\mathbf{r}_m) & \dots & \mathbf{E}_n(\mathbf{r}_m) \end{pmatrix}. \quad (17)$$

The number of rows in the matrix T_{nm} determines the accuracy of optical image reconstruction and the maximal size of the observation area. Based on the T_{nm} matrix, the incident wave front is formed (Fig. 22a), which ensures constructive interference in the near field and, correspondingly, a subwavelength focal spot, as shown in Fig. 22b.

Figure 23a presents the experimental setup for subwavelength optical visualization of an object in immediate contact with a defocusing superlens (the distance between the object and the lens is much less than the wavelength of light). Figures 23c–d show a reconstruction of the image of the initial object (Fig. 23b) without using and using matrix T_{nm}.

It is possible to improve the spatial resolution (within 30–50%) using a nonlinear interaction of the n-th order, because the point spread function $\mathrm{PSF}(x) \propto I^n(x)$, where $I(x)$ is the

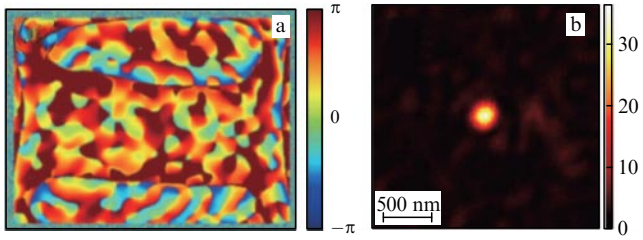

Figure 22. (Color online.) (a) Phase contrast of an incident wave front for forming a subwavelength focal spot (b) [183]. (Figure from Ref. [183] reproduced courtesy of © Springer Nature 2013.)

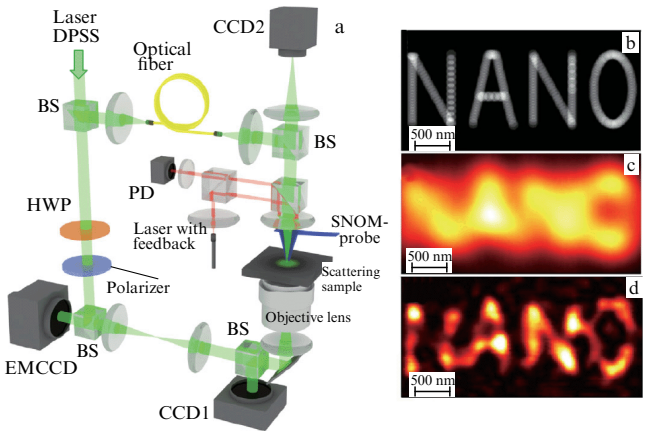

Figure 23. (Color online.) (a) Experimental setup for overcoming the diffraction limit based on a turbid medium. (b) Electron image of the structure obtained by lithography. (c, d) Reconstruction of the optical image without using and using a T matrix, respectively [183]. DPSS laser — diode-pumped solid-state laser, BS — beam splitter, HWP — half-wave plate, EMCCD — electron-multiplying charge-couple device, PD — quadrant photodiode. (Figure from Ref. [182] reproduced courtesy of © American Physical Society 2014.)

profile of the laser beam. Overcoming the diffraction limit is possible using masks for spatial modulation of light [187, 188] and induced decoherence with a ring-shaped laser beam [189]. Recently, methods of coherent anti-Stokes Raman high-order ($\chi^{(5)}$, $\chi^{(7)}$) scattering of light have been intensely developed [190–192].

6. Discussion

To date, the best developed and widely used approach is the use of scanning probe microscopes. In these devices, the image is formed by mechanical scanning of a thin needle, the tip size of which determines the resolution. An obvious drawback is the long duration of the image construction process, making the study of fast processes in real time impossible. Other methods use markers in the form of fluorescent particles or quantum dots. In these methods, the studied objects must be modified in a special way to make observations possible. Recently, STED microscopes and single molecule localization (SML) microscopes have been developed. With these devices, however, it is necessary to irradiate the samples with high-intensity beams, which may lead to sample damage, particularly unwanted in biology and medicine.

Although methods that require no mathematical processing of optical signals possess obvious substantial advantages, in the nearest future we expect computational methods and artificial intelligence to grow in importance for imaging

extremely small objects in a field of electromagnetic waves. An example of using frequency scanning and simple numerical algorithms is presented in Section 4.1 [142]. Another promising example of subwavelength imaging in real time using data array processing can be found in preprint [193]. In this method, the small-scale structure of the object is studied by measuring the field scattered to the far zone upon irradiation of the object with an incident field containing spatial superoscillations. The object structure is ultimately reconstructed by means of an artificial intelligence algorithm, which is trained by making comparisons with a field scattered by known objects.

Extremely promising are the conversion of subwavelength details of an object into a signal that varies in time and is transmitted using propagating waves [194], as well as the inversion of this signal in time for the purpose of subwavelength focusing [195–198].

Finally, it is impossible not to mention that in 2011 in Ref. [199] a remarkable property of a glass microsphere to form a magnified subwavelength image of objects located near the surface of the sphere was discovered experimentally. The image area is rather small, about 4 μm around the point of contact between the sphere and the substrate. However, this area is significantly larger than that covered by the best of known hyperlenses, to say nothing of the probes of near-field microscopes. Of course, a glass microsphere should not have significant irregularities in order to have the functionality of a hyperlens. Nevertheless, it is much cheaper to produce than a hyperlens [200]. At the same time, both the magnification of a subwavelength image and, which is most important, the spatial resolution in the glass microsphere are much better than in known hyperlenses. Namely, a resolution of $\lambda/8$ for dielectric objects [201] and $\lambda/15$ for objects of plasmonic metal [202] is experimentally achieved in lateral directions. For hyperlenses, as we saw above, this quantity in practice does not exceed a quarter of a wavelength. The magnification that can be practically achieved with hyperlenses is no greater than three times, whereas a microsphere provides a magnification of a few hundred times. Finally, the use of interferometric together with spectroscopic equipment offers the potential to reconstruct not only a two-dimensional but also a three-dimensional image with subwavelength resolution in the normal direction equal to $\lambda/10$ [203].

The mentioned effects make a glass microsphere a serious competitor for any metalens. However, the physics of subwavelength far-field imaging by a microsphere has been far from completely studied. Therefore, it is not clear which structures besides the microsphere already studied will work like an improved hyperlens and which will not.

Theoretically, a few physical mechanisms related to microsphere resonances or its resonant interaction with a plasmonic substrate were found, but they do not explain most of the experimental results. Some theoretical models of well-known experiments, for example, [204], do not hold up under scrutiny, as can be read in review [205]. Therefore, various particular models of subwavelength far-field imaging by a glass microsphere continue to be constructed. Thus, in recent paper [206], hypotheses of two possible mechanisms of the effect are presented, not related to any resonances. One of the hypotheses, the formation of a diffraction-free diverging beam of rays by the microsphere, is tested by numerical simulation. According to the literature, it is possible to conclude that, among all lines of research related to subwavelength imaging without mathematical processing of data arrays, dielectric microspheres attract the most interest from physicists. Papers on subwavelength imaging using fluorescent markers are mainly published in interdisciplinary and chemistry journals.

Nevertheless, in spite of all these new effects and achievements, the metalens remains a subject worth attention from the point of view of both fundamental and applied research. In our opinion, metalenses with subwavelength properties are worth a special detailed review.

First, both well-developed fluorescence nanoscopy and as yet only promising nanoscopy based on a glass microsphere are contact methods of imaging. In one case, the markers are to be applied directly to the object under study. In the other case, the microsphere must be positioned so that the object is sandwiched between it and the substrate. At the same time, a metalens is a thin film that forms a subwavelength image of an object in the transmitted field, i.e., on the other side of the film. Therefore, contact of the imaged object with any parts of the imaging system (except the metalens itself that serves as a substrate for the imaged object) is excluded. As shown in Ref. [131], image formation on the other side of the object is an important advantage of any metalens, particularly for medical applications.

Second, besides the metalens for subwavelength imaging, we considered metalenses that perform subwavelength focusing of an incident plane wave. However, the most interesting application has not been described above. This application, the most interesting in our opinion, a focusing metalens, is found in so-called metatronics [207]. Metatronics is a research field in photonics that links work aimed at creating an all-optical processor, memory devices, and other components of an all-optical computer of the near future. Here, we can mention, for instance, papers [207–212]. The literature on metatronics is vast and its volume is growing. Within metatronics, metallic, dielectric, and semiconductor nanoparticles (from nanospheres to nanowires) play the same role for light photons as lumped elements of common circuits do for current electrons. In addition, nanoparticles in metatronics serve as a base for optical nanodiodes, nanotransistors, etc. One of the most important tasks of metatronics is the focusing of wave beams carrying an optical signal onto these nanoparticles.

7. Conclusions

The creation of microscopes for observing extremely small objects has been and remains an important task for science and technology. The existence of the diffraction limit of resolution in conventional optical devices requires novel approaches using new physical principles. There are many different methods, each having its area of application, advantages, and drawbacks.

In the present review, we talked about the approaches that can help to overcome disadvantages of known subwavelength microscopy instruments. Of course, these methods also have their limitations and disadvantages, but opening up the possibility of observing nanoobjects in real time without irradiation by strong fields is giving rise to great scientific and practical interest.

The work was carried out with financial support from the Russian Foundation for Basic Research (RFBR) within research project no. 19-12-50348. S.S.Kh. is grateful to the Russian Science Foundation (RSF), grant no. 19-12-00066, for support in writing the sections on Veselago–Pendry metalenses and superlenses based on turbid media.

References

1. Born M, Wolf E *Principles of Optics* (Oxford: Pergamon Press, 1965); Translated into Russian: *Osnovy Optiki* (Moscow: Nauka, 1973)
2. Niz'ev V G *Phys. Usp.* **45** 553 (2002); *Usp. Fiz. Nauk* **172** 601 (2002)
3. Novotny L, Hecht B *Principles of Nano-Optics* (Cambridge: Cambridge Univ. Press, 2006); Translated into Russian: *Osnovy Nanooptiki* (Moscow: Fizmatlit, 2009)
4. Narimanov E *Adv. Photon.* **1** 056003 (2019)
5. So S et al. *Appl. Spectrosc. Rev.* **53** 290 (2018)
6. Remnev M A, Klimov V V *Phys. Usp.* **61** 157 (2018); *Usp. Fiz. Nauk* **188** 169 (2018)
7. Synge E H *Philos. Mag. 7* **6** 356 (1928)
8. Betzig E, Trautman J K *Science* **257** 189 (1992)
9. Hecht B et al. *J. Chem. Phys.* **112** 7761 (2000)
10. Verma P *Chem. Rev.* **117** 6447 (2017)
11. Zrimsek A B et al. *Chem. Rev.* **117** 7583 (2017)
12. Mauser N, Hartschuh A *Chem. Soc. Rev.* **43** 1248 (2014)
13. Deckert-Gaudig T et al. *Chem. Soc. Rev.* **46** 4077 (2017)
14. Dazzi A, Prater C B *Chem. Rev.* **117** 5146 (2017)
15. Huber A J et al. *Nat. Nanotechnol.* **4** 153 (2009)
16. Lee J et al. *Nature* **568** 78 (2019)
17. Betzig E et al. *Science* **313** 1642 (2006)
18. Rust M J, Bates M, Zhuang X *Nat. Meth.* **3** 793 (2006)
19. Gustafsson M G L *J. Microsc.* **198** 82 (2000)
20. Hell S W *Nat. Biotechnol.* **21** 1347 (2003)
21. Harke B et al. *Opt. Express* **16** 4154 (2008)
22. Mandelstam L I *Lektsii po Optike, Teorii Otnositel'nosti i Kvantovoi Mekhanike* (Lectures on Optics, Relativity Theory, and Quantum Mechanics) (Moscow: Nauka, 1972)
23. Sivukhin D V *Opt. Spektrosk.* **3** 308 (1957)
24. Veselago V G *Sov. Phys. Usp.* **10** 509 (1968); *Usp. Fiz. Nauk* **92** 517 (1967)
25. Pendry J B *Phys. Rev. Lett.* **85** 3966 (2000)
26. Osipov A V, Tretyakov S A *Modern Electromagnetic Scattering Theory with Applications* (Chichester: Wiley, 2017)
27. Klimov V V *JETP Lett.* **89** 229 (2009); *Pis'ma Zh. Eksp. Teor. Fiz.* **89** 270 (2009)
28. Klimov V V *Nanoplasmonics* (Singapore: Pan Stanford Publ., 2014)
29. Brongersma M L, Kik P G (Eds) *Surface Plasmon Nanophotonics* (Springer Series in Optical Sciences, Vol. 131) (Dordrecht: Springer, 2007)
30. Zhang X et al., in *Surface Plasmon Nanophotonics* (Springer Series in Optical Sciences, Vol. 131, Eds M L Brongersma, P G Kik) (Dordrecht: Springer, 2007) p. 105
31. Casse B D F et al. *Opt. Lett.* **34** 1994 (2009)
32. Wood B, Pendry J B, Tsai D P *Phys. Rev. B* **74** 115116 (2006)
33. Podolskiy V A, Kuhta N A, Milton G W *Appl. Phys. Lett.* **87** 231113 (2005)
34. Guzatov D V, Klimov V V *Quantum Electron.* **44** 873 (2014); *Kvantovaya Elektron.* **44** 873 (2014); Guzatov D V, Klimov V V *Quantum Electron.* **44** 1112 (2014); *Kvantovaya Elektron.* **44** 1112 (2014)
35. Fang N et al. *Science* **308** 534 (2005)
36. Hong F, Blaikie R *Adv. Opt. Mater.* **7** 1801653 (2019)
37. Silin R A *Opt. Spektrosk.* **44** 198 (1978)
38. Silin R A *Neobyknovennye Zakony Prelomleniya i Otrazheniya* (Unusual Laws of Refraction and Reflection) (Moscow: Fazis, 2002)
39. Smith D R et al. *Phys. Rev. Lett.* **84** 4184 (2000)
40. Capolino F (Ed.) *Theory and Phenomena of Metamaterials* (Boca Raton, FL: CRC Press. Taylor and Francis, 2009)
41. Xiao S et al. *Nature* **466** 735 (2010)
42. Pendry J B et al. *Phys. Rev. Lett.* **76** 4773 (1996)
43. Lagarkov A N et al. *J. Magn. Magn. Mater.* **258 – 259** 161 (2003)
44. Morits D, Simovski C *J. Opt.* **14** 125102 (2012)
45. Paniagua-Domínguez R, Abujetas D R, Sánchez-Gil J A *Sci. Rep.* **3** 1507 (2013)
46. Capolino F (Ed.) *Applications of Metamaterials* (Boca Raton, FL: CRC Press, 2009)
47. Cubukcu E et al. *Nature* **423** 604 (2003)
48. Cai W, Genov D A, Shalaev V M *Phys. Rev. B* **72** 193101 (2005)
49. Cai W, Shalaev V *Optical Metamaterials*: *Fundamentals and Applications* (New York: Springer, 2010)
50. Smith D R et al. *Phys. Rev. E* **71** 036617 (2005)
51. Kharintsev S S et al. *Nanoscale* **11** 7710 (2019)
52. Kharintsev S S *Opt. Lett.* **44** 5909 (2019)
53. Kharintsev S S et al. *ACS Appl. Mater. Interfaces* **12** 3862 (2020)
54. Belov P A, Simovski C R, Ikonen P *Phys. Rev. B* **71** 193105 (2005)
55. Ikonen P et al. *Phys. Rev. B* **73** 073102 (2006)
56. Belov P A, Hao Y, Sudhakaran S *Phys. Rev. B* **73** 033108 (2006)
57. Belov P A, Hao Y *Phys. Rev. B* **73** 113110 (2006)
58. Belov P A, Silveirinha M G *Phys. Rev. E* **73** 056607 (2006)
59. Zhao Y, Belov P A, Hao Y *Opt. Express* **14** 5154 (2006)
60. Belov P A et al. *Appl. Phys. Lett.* **89** 262109 (2006)
61. Silveirinha M G, Belov P A, Simovski C R *Phys. Rev. B* **75** 035108 (2007)
62. Shvets G et al. *Phys. Rev. Lett.* **99** 053903 (2007)
63. Silveirinha M G, Belov P A, Simovski C R *Opt. Lett.* **33** 1726 (2008)
64. Casse B D F et al. *Appl. Phys. Lett.* **96** 023114 (2010)
65. Simovski C R et al. *Adv. Mater.* **24** 4229 (2012)
66. Belov P A et al. *Phys. Rev. B* **77** 193108 (2008)
67. Belov P A et al. *Phys. Rev. B* **67** 113103 (2003)
68. Poddubny A et al. *Nat. Photon.* **7** 948 (2013)
69. Maslovski S I, Silveirinha M G *Phys. Rev. B* **80** 245101 (2009)
70. Luo C et al. *Phys. Rev. B* **68** 045115 (2003)
71. Silveirinha M G *Phys. Rev. E* **73** 046612 (2006)
72. Forouzmand A, Bernety H M, Yakovlev A B *Phys. Rev. B* **92** 085402 (2015)
73. Ono A, Kato J, Kawata S *Phys. Rev. Lett.* **95** 267407 (2005)
74. Rahman A, Belov P A, Hao Y *Phys. Rev. B* **82** 113408 (2010)
75. Rahman A et al. *J. Nanophoton.* **5** 051601 (2011)
76. Kawata S, Ono A, Verma P *Nat. Photon.* **2** 438 (2008)
77. Voroshilov P M et al. *J. Nanophoton.* **5** 053516 (2011)
78. Webb K J, Yang M *Opt. Lett.* **31** 2130 (2006)
79. Elsayad K, Heinze K G *PloS ONE* **4** e7963 (2009)
80. Li T et al. *Opt. Express* **25** 13588 (2017)
81. Kotyński R, Stefaniuk T *J. Opt. A* **11** 015001 (2009)
82. Chigrin D N et al. *Opt. Express* **11** 1203 (2003)
83. Li Z-Y, Lin L-L *Phys. Rev. B* **68** 245110 (2003)
84. Kuo C-H, Ye Z *Phys. Rev. E* **70** 056608 (2004)
85. Chien H-T et al. *Phys. Rev. B* **70** 113101 (2004)
86. Parimi P V et al. *Nature* **426** 404 (2003)
87. Foteinopoulou S, Soukoulis C M *Phys. Rev. B* **67** 235107 (2003)
88. Cubukcu E et al. *Phys. Rev. Lett.* **91** 207401 (2003)
89. Moussa R et al. *Phys. Rev. B* **71** 085106 (2005)
90. Savo S, Di Gennaro E, Andreone A *Opt. Express* **17** 19848 (2009)
91. Matsumoto T, Eom K-S, Baba T *Opt. Lett.* **31** 2786 (2006)
92. Fabre N et al. *Phys. Rev. Lett.* **101** 073901 (2008)
93. Vlasov Yu A, Moll N, McNab S J *Opt. Lett.* **29** 2175 (2004)
94. Caase B D F et al. *Opt. Lett.* **34** 1994 (2009)
95. Shi P, Huang K, Li Y *J. Opt. Soc. Am. A* **28** 2171 (2011)
96. Dorrani Z, Mansouri-Birjandi A *Int. J. Comput. Sci. Issues* **9** (3) 57 (2012)
97. Zakrzewski A, Patela S *Sensors Actuat. A* **256** 51 (2017)
98. Matsumoto T, Fujita S, Baba T *Opt. Express* **13** 10768 (2005)
99. Ouerghi F et al. *J. Lightwave Technol.* **27** 3269 (2009)
100. Belov P A et al. *Appl. Phys. Lett.* **97** 191905 (2010)
101. Yang K Y et al. *Phys. Rev. B* **86** 075309 (2012)
102. Ghoshroy A et al. *Opt. Lett.* **43** 1810 (2018)
103. Narimanov E E, Shalaev V M *Nature* **447** 266 (2007)
104. Jacob Z, Alekseyev L V, Narimanov E *Opt. Express* **14** 8247 (2006)
105. Salandrino A, Engheta N *Phys. Rev. B* **74** 075103 (2006)
106. Liu Z et al. *Science* **315** 1686 (2007)
107. Zhang X, Liu Z *Nat. Mater.* **7** 435 (2008)
108. Kildishev A V, Narimanov E E *Opt. Lett.* **32** 3432 (2007)
109. Smith E J et al. *Appl. Phys. Lett.* **95** 083104 (2009)
110. Tsang M, Psaltis D *Phys. Rev. B* **77** 035122 (2008)
111. Han S et al. *Nano Lett.* **8** 4243 (2008)
112. Kildishev A V, Shalaev V M *Opt. Lett.* **33** 43 (2008)
113. Li J et al. *Opt. Lett.* **34** 3128 (2009)
114. Wang W et al. *Opt. Express* **16** 21142 (2008)
115. Lee H et al. *Opt. Express* **15** 15886 (2007)
116. Rho J et al. *Nat. Commun.* **1** 143 (2010)
117. Kerbst J et al. *Appl. Phys. Lett.* **99** 191905 (2011)

118. Schwaiger S et al. *Phys. Rev. Lett.* **102** 163903 (2009)
119. Li G X et al. *J. Appl. Phys.* **104** 096103 (2008)
120. Li P et al. *Nat. Commun.* **6** 7507 (2015)
121. Ikonen P et al. *Appl. Phys. Lett.* **91** 104102 (2007)
122. Zhao Y et al. *New J. Phys.* **12** 103045 (2010)
123. Shvets G, Trendafilov S *Proc. SPIE* **6641** 66410V (2007)
124. Tuniz A et al. *Nat. Commun.* **4** 2706 (2013)
125. Radu X, Lapeyronnie A, Craeye C *Electromagnetics* **28** 531 (2008)
126. Radu X, Garray D, Craeye C *Metamaterials* **3** 90 (2009)
127. Vovchuk D, Kosulnikov S, Simovski C *Opt. Express* **26** 17988 (2018)
128. Glybovski S B et al. *Phys. Rep.* **634** 1 (2016)
129. Khorasaninejad M, Capasso F *Science* **358** eaam8100 (2017)
130. Lalanne P, Chavel P *Laser Photon. Rev.* **11** 1600295 (2017)
131. Mollaei M S M, Simovski C *Phys. Rev. B* **100** 205426 (2019)
132. Maslovski S, Tretyakov S, Alitalo P *J. Appl. Phys.* **96** 1293 (2004)
133. Freire M J, Marqués R *Appl. Phys. Lett.* **86** 182505 (2005)
134. Sydoruk O, Shamonina E, Solymar L *Microwave Opt. Technol. Lett.* **49** 2228 (2007)
135. Sydoruk O et al. *J. Appl. Phys.* **101** 073903 (2007)
136. Simovski C R, Viitanen A J, Tretyakov S A *Phys. Rev. E* **72** 066606 (2005)
137. Alitalo P et al. *Phys. Rev. B* **74** 235425 (2006)
138. Mateo-Segura C et al. *Opt. Lett.* **34** 2333 (2009)
139. Maslovski S, Tretyakov S *J. Appl. Phys.* **94** 4241 (2003)
140. Maslovski S, Tretyakov S *New J. Phys.* **14** 035007 (2012)
141. Pendry J B *Science* **322** 71 (2008)
142. Maslovski S, Alitalo P, Tretyakov S *J. Appl. Phys.* **104** 103109 (2008)
143. Marks D, Carney P S *Opt. Lett.* **30** 1870 (2005)
144. Merlin R *Science* **317** 927 (2007)
145. Fu Y et al. *Appl. Phys. Lett.* **91** 061124 (2007)
146. Mote R G et al. *Opt. Express* **16** 9554 (2008)
147. Imani M F, Grbic A *Metamaterials* **4** 104 (2010)
148. Grbic A et al. *Proc. IEEE* **99** 1806 (2011)
149. Imani M F, Grbic A *IEEE Antennas Wirel. Propag. Lett.* **8** 421 (2009)
150. Imani M F, Grbic A *Appl. Phys. Lett.* **95** 111107 (2009)
151. Grbic A, Jiang L, Merlin R *Science* **320** 511 (2008)
152. Imani M F, Grbic A, in *2009 IEEE Antennas and Propagation Society Intern. Symp.* (Piscataway, NJ: IEEE, 2009) https://doi.org/10.1109/APS.2009.5172270
153. Imani M F, Grbic A *IEEE Trans. Microwave Theory Tech.* **58** 3982 (2010)
154. Berry M V, Moiseyev N *J. Phys. A* **47** 315203 (2014)
155. Aharonov Y, Albert D Z, Vaidman L *Phys. Rev. Lett.* **60** 1351 (1988)
156. Aharonov Y et al. *Phys. Rev. Lett.* **64** 2965 (1990)
157. Berry M V, in *Quantum Coherence and Reality: in Celebration of the 60th Birthday of Yakir Aharonov. Proc. of the Intern. Conf. on Fundamental Aspects of Quantum Theory, Univ. of South Carolina, Columbia, 10–12 December 1992* (Eds J S Anandan, J L Safko) (Singapore: World Scientific, 1995) p. 55
158. Zheludev N I *Nat. Mater.* **7** 420 (2008)
159. Wong A M H, Eleftheriades G V *IEEE Antennas Wirel. Propag. Lett.* **9** 315 (2010)
160. Makris K G, Psaltis D *Opt. Lett.* **36** 4335 (2011)
161. Cohen E et al. *Nat. Rev. Phys.* **1** 437 (2019)
162. Gbur G *Nanophotonics* **8** 205 (2019)
163. Berry M V, Popescu S *J. Phys. A* **39** 6965 (2006)
164. Huang F M et al. *J. Opt. A* **9** S285 (2007)
165. Huang F M et al. *Appl. Phys. Lett.* **90** 091119 (2007)
166. Huang F M et al. *Nano Lett.* **8** 2469 (2008)
167. Huang F M, Zheludev N I *Nano Lett.* **9** 1249 (2009)
168. Rogers E T F et al. *Nat. Mater.* **11** 432 (2012)
169. Rogers E T F, Zheludev N I *J. Opt.* **15** 094008 (2013)
170. Huang K et al. *Laser Photon. Rev.* **157** 152 (2014)
171. Rogers E T F et al. *Biophys. J.* **108** (Suppl. 1) 479a (2015)
172. Yuan G et al., in *Conf. on Lasers and Electro-Optics* (OSA Technical Digest, online) (Washington, DC: Optica Publ. Group, 2018) paper FM3J.2, https://doi.org/10.1364/CLEO_QELS.2018.FM3J.2
173. Yuan G H, Rogers E T F, Zhelude N I *Light Sci. Appl.* **6** e17036 (2017)
174. Wong A M H, Eleftheriades G V *Sci. Rep.* **5** 8449 (2015)
175. Dong X H et al. *Optica* **4** 1126 (2017)
176. Rogers K S et al. *Opt. Express* **26** 8095 (2018)
177. Yuan G et al. *Phys. Rev. Appl.* **11** 064016 (2019)
178. Wintz D et al. *Nano Lett.* **15** 3585 (2015)
179. Khorasaninejad M et al. *Nano Lett.* **16** 4595 (2016)
180. Tang D et al. *Laser Photon. Rev.* **9** 713 (2015)
181. Rogers E T et al. *Biophys. J.* **112** 186a (2017)
182. Park C et al. *Phys. Rev. Lett.* **113** 113901 (2014)
183. Park J-H et al. *Nat. Photon.* **7** 454 (2013)
184. Wiersma D S *Nat. Photon.* **7** 188 (2013)
185. Song P et al. *Opt. Lett.* **44** 3645 (2019)
186. van Putten E G et al. *Phys. Rev. Lett.* **106** 193905 (2011)
187. Raghunathan V, Potma E O *J. Opt. Soc. Am. A* **27** 2365 (2010)
188. Kim H, Bryant G W, Stranick S J *Opt. Express* **20** 6042 (2012)
189. Silva W R, Graefe C T, Frontiera R R *ACS Photon.* **3** 79 (2015)
190. Gong L et al. *Nat. Photon.* **14** 115 (2020)
191. Cho M et al. *J. Chem. Phys.* **112** 2082 (2000)
192. Blank D A, Kaufman L J, Fleming G R *J. Chem. Phys.* **111** 3105 (1999)
193. Pu T, Ou J-Y, Papasimakis N, Zheludev N I, arXiv:2001.01068
194. Lemoult F et al. *Phys. Rev. Lett.* **104** 203901 (2010)
195. Lerosey G et al. *Phys. Rev. Lett.* **92** 193904 (2004)
196. Lerosey G et al. *Science* **315** 1120 (2007)
197. Lemoult F, Fink M, Lerosey G *Nat. Commun.* **3** 889 (2012)
198. Mosk A P et al. *Nat. Photon.* **6** 283 (2012)
199. Wang Z et al. *Nat. Commun.* **2** 218 (2011)
200. Lecler S et al. *Sci. Rep.* **9** 4725 (2019)
201. Sundaram V M, Wen S-B *Appl. Phys. Lett.* **105** 204102 (2014)
202. Cang H et al. *Nat. Commun.* **6** 7942 (2015)
203. Kassamakov I et al. *Sci. Rep.* **7** 3683 (2017)
204. Yang H et al. *Nano Lett.* **16** 4862 (2016)
205. Maslov A V, Astratov V N *Phys. Rev. Appl.* **11** 064004 (2019)
206. Heydarian R, Simovski C R *J. Opt.* **22** 075002 (2020)
207. Engheta N *Phys. World* **23** (9) 31 (2010)
208. Singh P et al. *Adv. Opt. Technol.* **2014** 275083 (2014)
209. Piccione B et al. *Nat. Nanotechnol.* **7** 640 (2012)
210. Li W et al. *Nano Lett.* **14** 955 (2014)
211. Chen W et al. *Science* **341** 768 (2013)
212. Kuramochi E, Notomi M *Nat. Photon.* **9** 712 (2015)